A Charge Detector for Measurement of Ionic Solutes.

Bingcheng Yang, Yongjing Chen, Masanobu Mori, Shin-Ichi Ohira,
Abul K. Azad and Purnendu K. Dasgupta*

Department of Chemistry and Biochemistry
University of Texas, 700 Planetarium Place, Arlington, TX 76019-0065.

Kannan Srinivasan
Dionex Corporation, 1228 Titan way, Sunnyvale, CA 94086

Supplementary Information

Construction of Bead-based Charge Detector (ChD-B)

The through-channels of both arms of a 10-32 4-way cross fitting (P-730, Upchurch) were bored out for 1.6 mm o.d. PEEK tubing to just pass through. For each of two segments of 0.5 mm i.d., 1.6 mm o.d. PEEK tubing, the terminal bore at one end was widened to 0.9 mm to a depth of ~1 mm. Ion exchange resin beads (Rexyn 101 H^+-type for the cation exchange resin (CER) and Dowex AG -2X8 Cl^-form for the anion exchange resin (AER)) were dried in a desiccator and hand-picked to obtain resin beads in the 0.8 -0.85 mm size range. One CER and one AER bead were placed in the respective drilled out cavities in the PEEK tube and wetted with water whereupon they expanded and lodged tightly in the cavity. As shown in Figure 1, these two bead-bearing tubes were placed opposite each other (fixed in place with 10-32 nuts and ferrules, not shown), with the distance between CER and AER being ~ 0.4 mm. Water inlet and eluent outlet tubes were then similarly connected. At the back side, each bead-bearing tube was cut off essentially flush with the back of the holding nuts and a small segment of Tygon sleeve tubing put over the ends of the 1.6 mm o.d. PEEK tubes. A blunt-ended platinum needle (0.25 mm i.d., 0.45 mm o.d.; 26 ga., 25 mm long, P/N 21126 PT 3, Hamilton Co. Reno, NV) was put in all the way into the PEEK tubing, just touching the bead. The exit of the Pt Needle from the Tygon tube was sealed with hot-melt adhesive. The Pt-needle functioned both as the electrode and the liquid inlet tube; the liquid outlet was provided by a 0.25 mm. i.d., 0.51 mm o.d. PEEK tube (P/N 1542, Upchurch) breaching the Tygon tube wall, and affixed in place with adhesive. The nominal internal volume of the device, without considering the space that the protrusion of the spherical beads may consume, is ~3.2 μL.

Dionex Suppresor Design

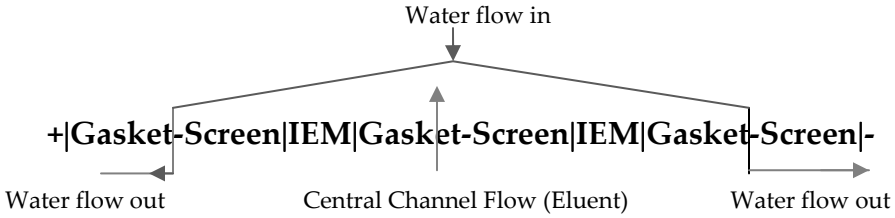

Scheme I

The screens referred to above break up flow laminarity to enhance mass transport to the membranes.

The basic suppressor design of the above scheme and shown in Figure S1 is described below. Each outer compartment contains a platinum electrode in contact with a flow channel which consists of a gasketed screen with an ion exchange membrane (IEM) on the other side of the screen. The central compartment contains an IEM on both sides. The screens have an integral proprietary soft polymeric gasket material, the portion of the screens not covered by the gasket define the fluidic pathway. The purpose of the screen structure in each flow path is to break up flow laminarity and improve mass transfer to the membrane. The screens in the outer channels are also ion exchange functionalized similar to the membranes they are adjacent to, thus effectively increasing the ion exchange capacities of the membranes. Water or a regenerant solution comes in and splits into two parts, flowing through each of the two outer channels to waste while the central channel flow proceeds independently. Detailed physical design of these devices is complex. The unfamiliar reader is referred to the original papers describing such designs,[1,2] the patents,[3,4]and a more recent review.[5] The hardware used to hold the assembly together is shown in Figure S2.

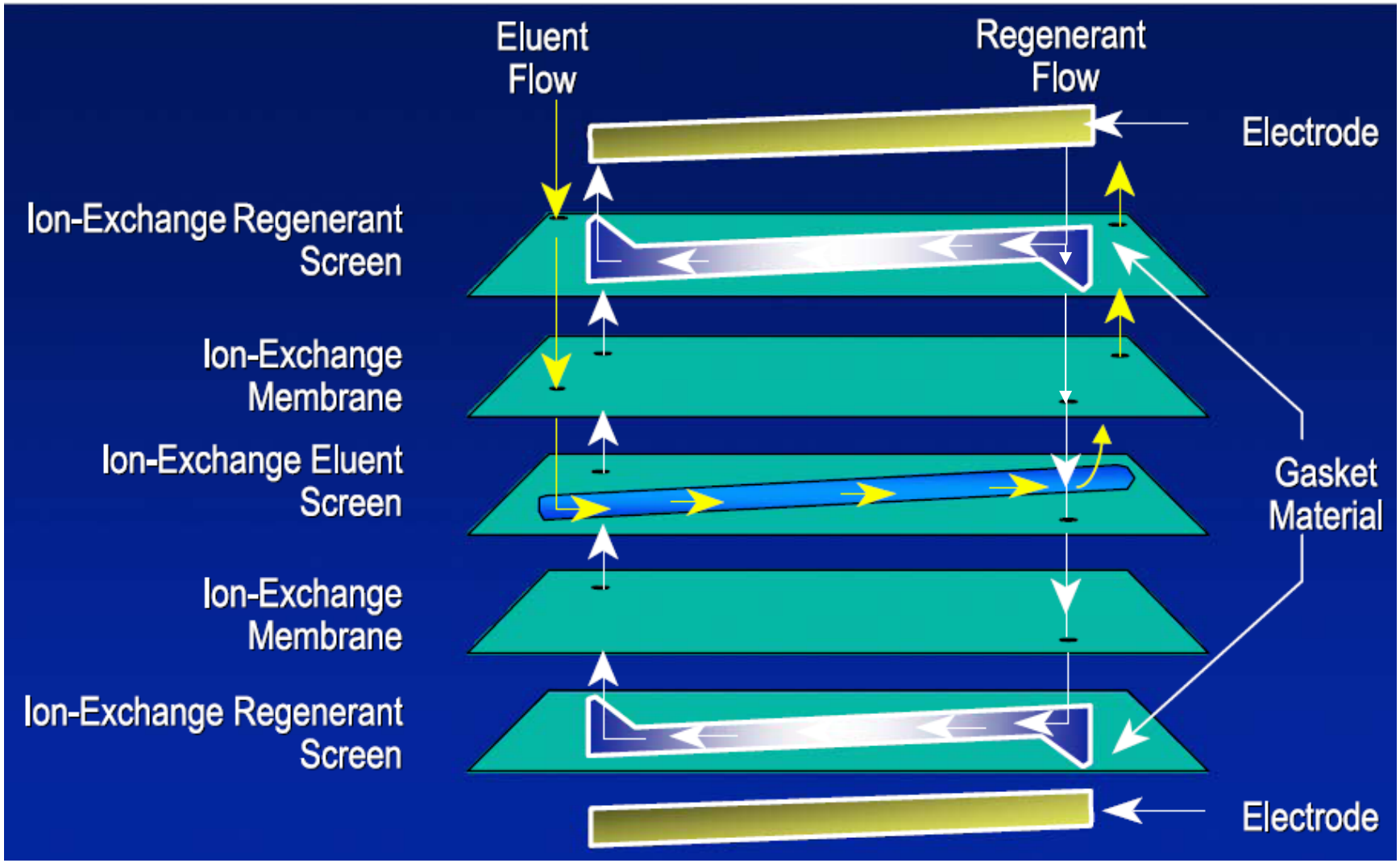

Figure S1. Dionex electrical suppressor configuration.[6]

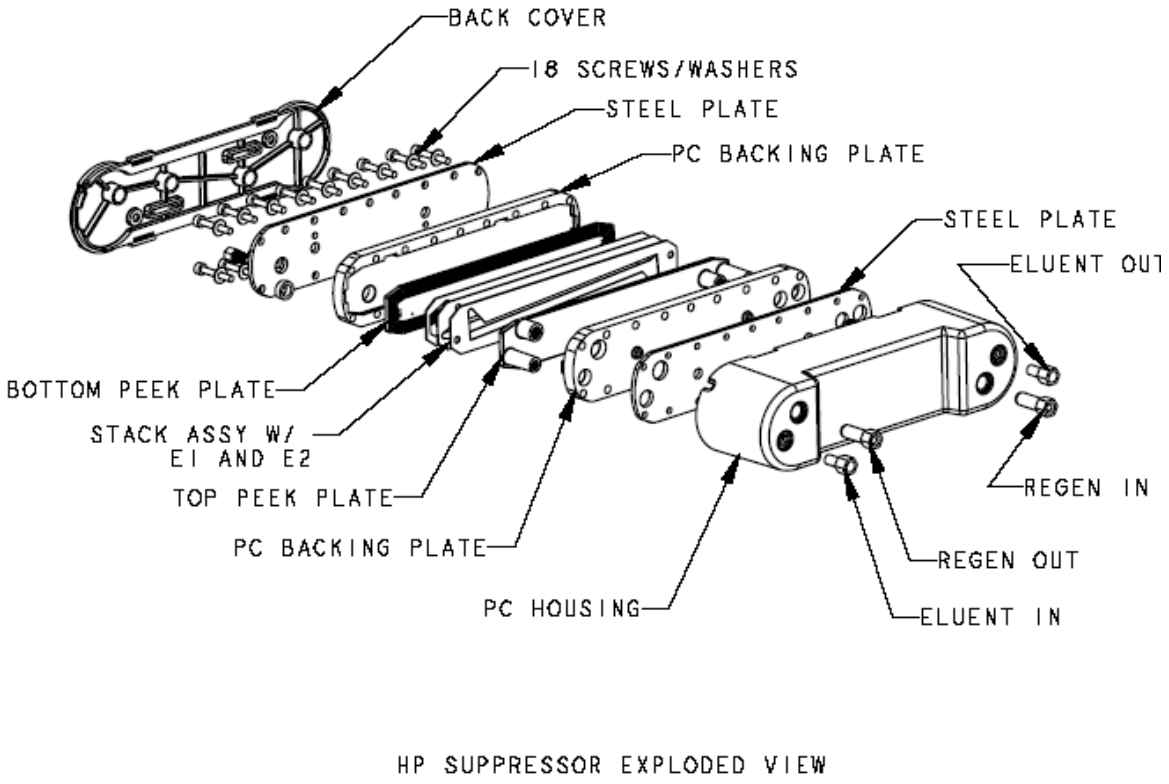

Figure S2. Electrical Suppressor Assembly Hardware.

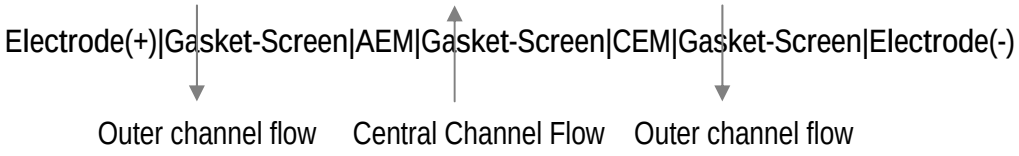

Scheme II

To construct a ChD, conventional suppressor hardware must be modified to accomplish this independent flow scheme as shown above in Scheme II.

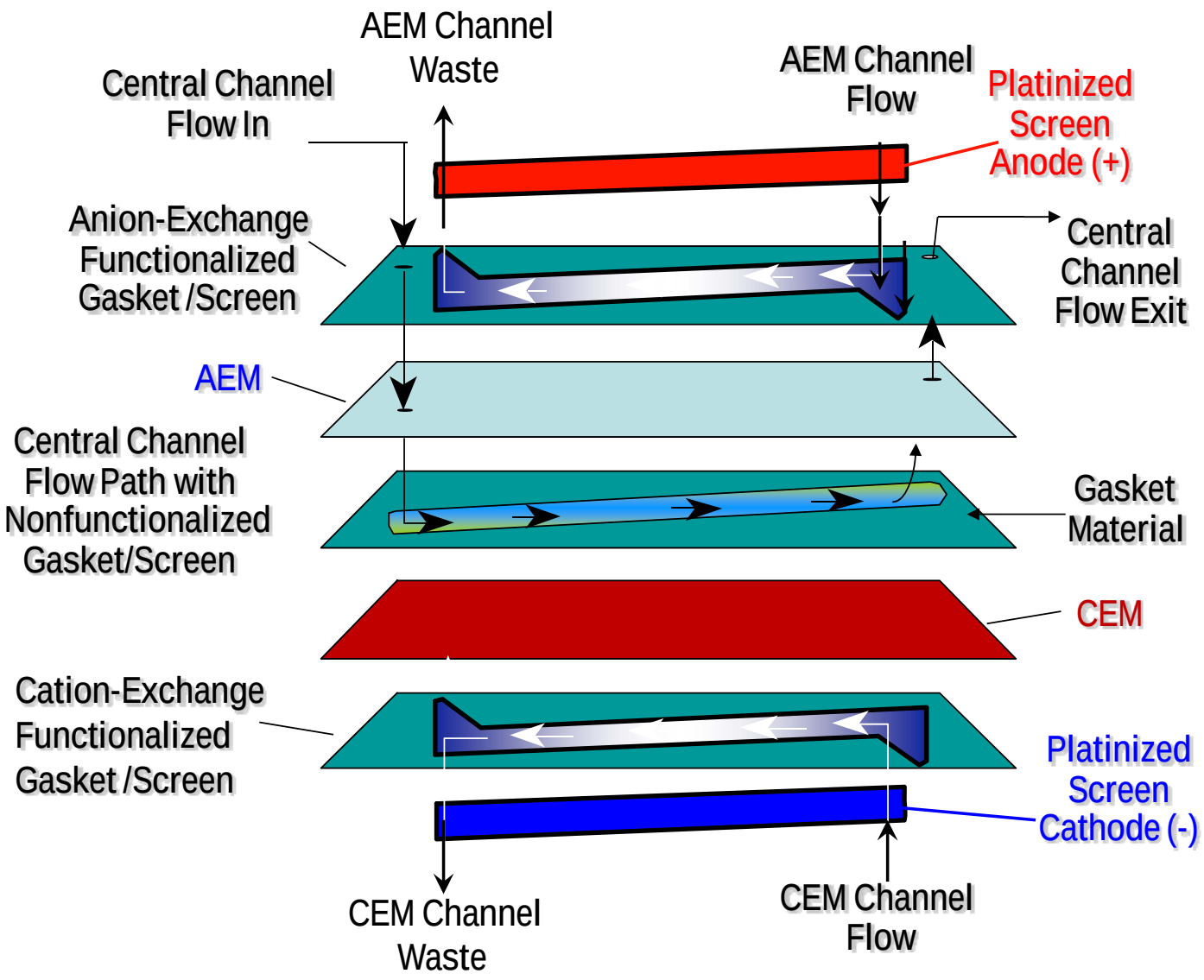

Figure S3. Membrane based charge detector with screen separated electrodes (MSSE devices)

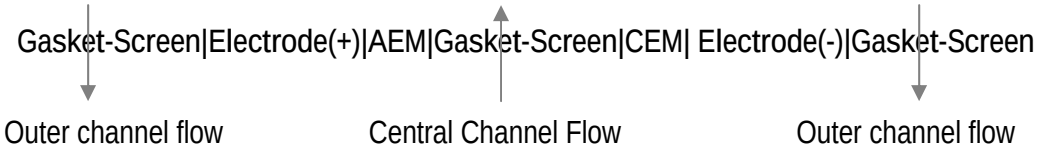
Gasket-Screen|Electrode(+)|AEM|Gasket-Screen|CEM| Electrode(-)|Gasket-Screen
Outer channel flow
Central Channel Flow
Outer channel flow

Scheme III

Details of screens and electrodes for membrane devices.

We use polyethylene (PE) monofilament screens (410 mesh, approximately 500 μm thick) that are radiation grafted and then appropriately ion exchange functionalized in the outer channels. The central channel contains a 250 μm thick 140 mesh unmodified PE screen. The IEMs are 75 or 125 μm thick poly(tetrafluoroethylene) films that are radiation grafted and then ion exchange functionalized;[7] the ion exchange capacities are ~1.2-2 meq/g. The entire assembly is placed between two PEEK plates that have appropriate fittings to facilitate fluidic inlet and outlet for the three independent channels. The platinized screen electrodes are connected to platinum wires that are routed via orifices in the PEEK plate to the exterior of the device.

Current to Voltage Conversion and Data Acquisition.

Current-to-Voltage conversion was carried out with either (a) model 427A current amplifier (www.keithley.com), (b) National Instruments NI USB 4065 $6^1/_2$-digit multimeter (www.ni.com) (c) a homebuilt converter based on a FET input operational amplifier (TL082, www.ti.com), (d) a homebuilt converter based on an electrometer grade operational amplifier (OPA128, www.ti.com) or (e) Stanford Research System-low-noise current preamplifier (Model SR570). The best performance was observed with d and e, which generally provided 1.5-2x better S/N than b. The data were recorded after current to voltage conversion (see below) with either a 12–bit A/D card (PC-CARD-DAS16/12AO, www.measurementcomputing.com) at 1 Hz or, when using the membrane based devices, with the Chromeleon™ data system (www.dionex.com) at 5 Hz.

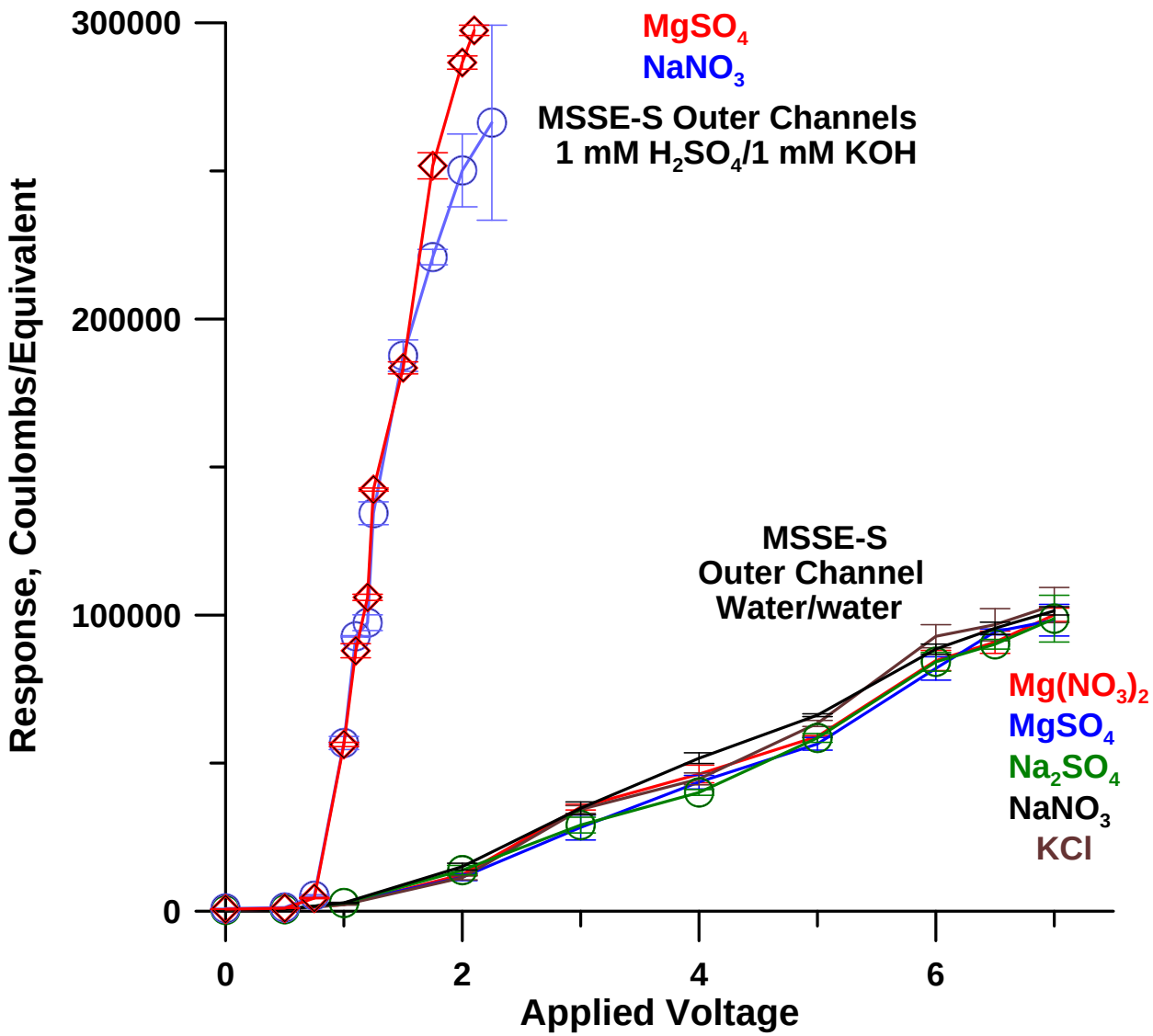

Figure S4. Response on an equivalent basis is virtually identical for a variety of strong electrolytes (1.32 neq) injected in this example in a MSSE-S device, across a range of applied voltages and whether water/water or dilute acid/base are used as CEM/AEM electrolytes. The latter dramatically increases the response but it affects the different analytes in the same manner. Error bars in this and all subsequent figures indicate ±1 standard deviation for three to five measurements (typically four) at each point. In some cases error bars are smaller than the dimensions of the symbols plotted and cannot be seen.

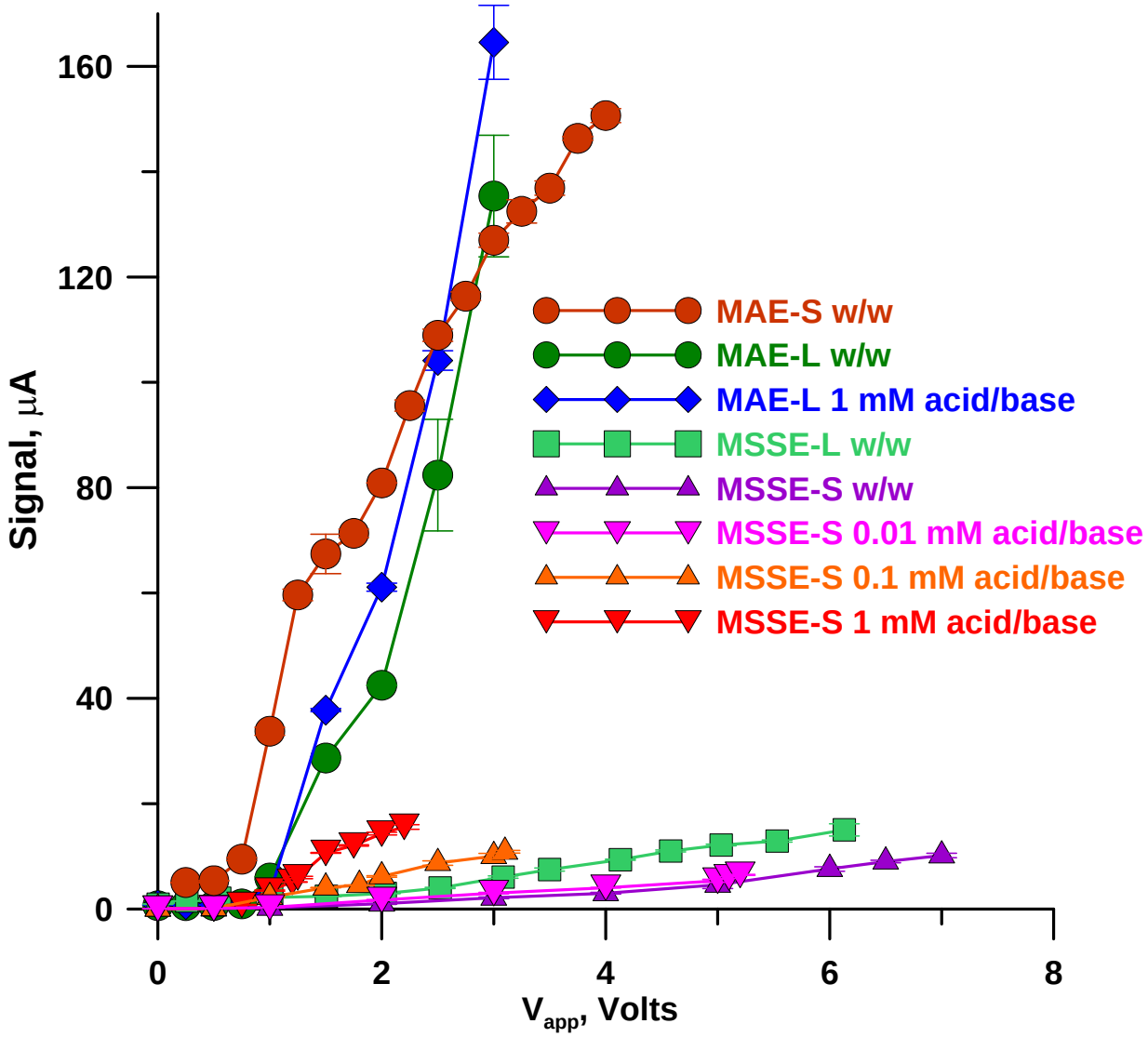

Figure S5. Signal height in μA shown for various membrane based ChD devices operated with CEM/AEM channels water/water or acid/base. For acid 0.01, 0.1, or 1.0 mM H_2SO_4 was used, the same molar concentrations of KOH were used as the corresponding base. Injection volumes of 50 μM $NaNO_3$ were 54 and 26 μL and the central channel flow rate 1000 and 200 μL/min, respectively for type -L and –S devices.

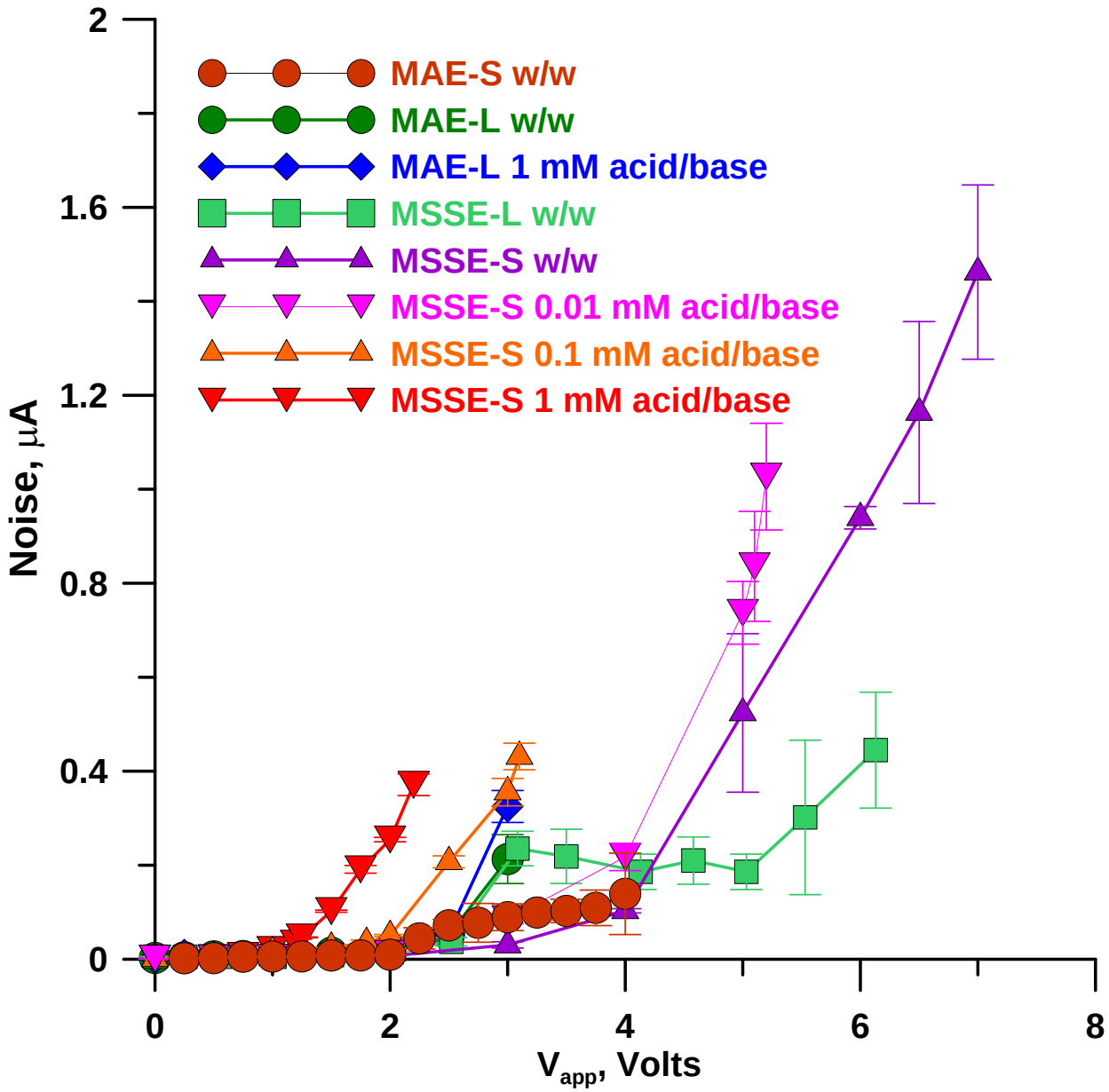

Figure S6. Background noise for the experiments in the previous figure (Figure S5).

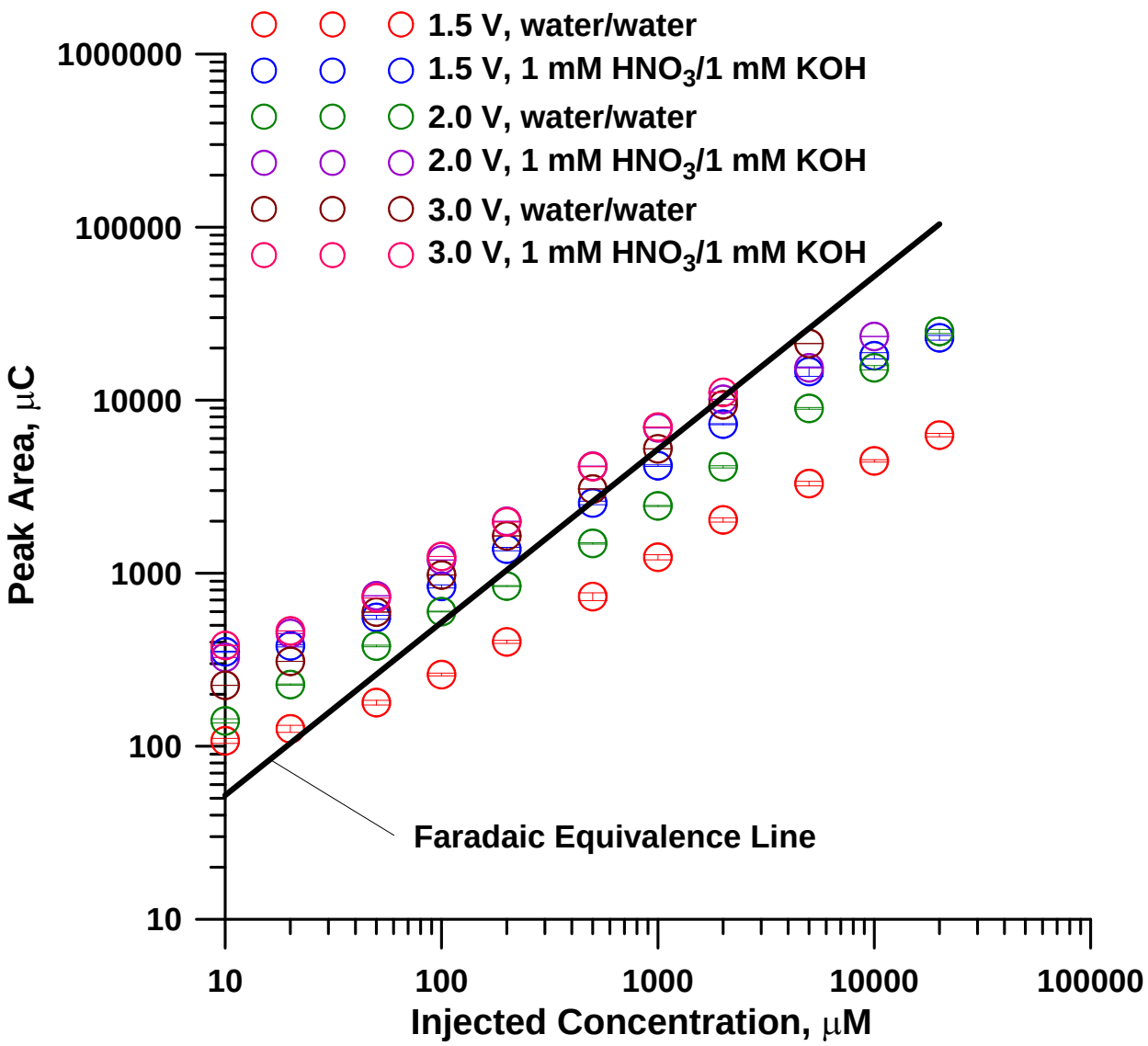

Figure S7. Enlarged color version of Figure 7(b). Calibration behavior for different injected concentrations of KNO_3 over a large concentration range. Device MAE-L operated with different fluid compositions in the CEM/AEM outer channels.

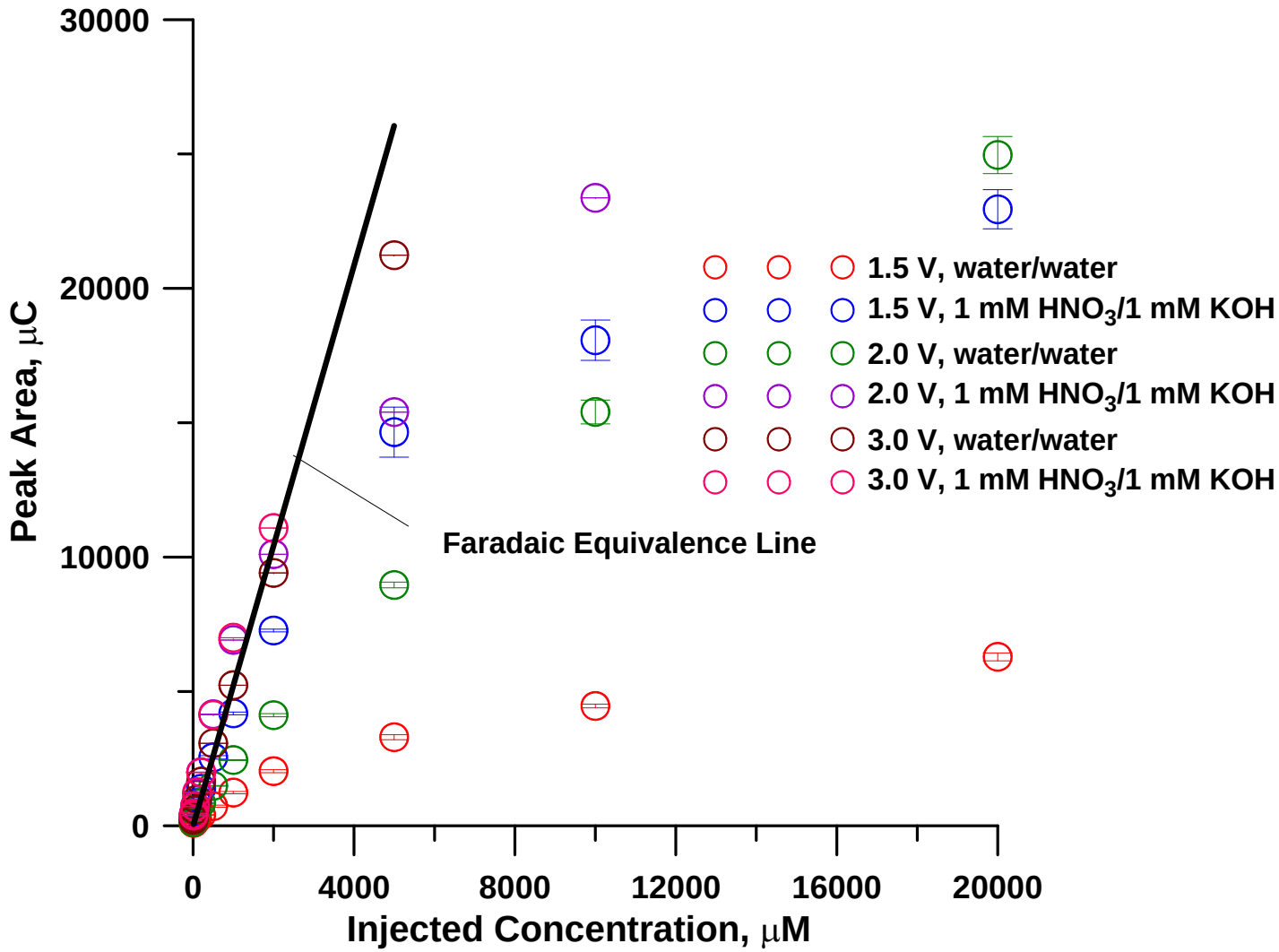

Figure S8. Linear abscissa ordinate version of the previous figure (Figure S7). The response is obviously nonlinear at V_{app} = 1.5V and 2V. However, Figures S9-S11 (that follow) show that over isolated decadal concentration spans, linear behavior can be assumed without significant error.

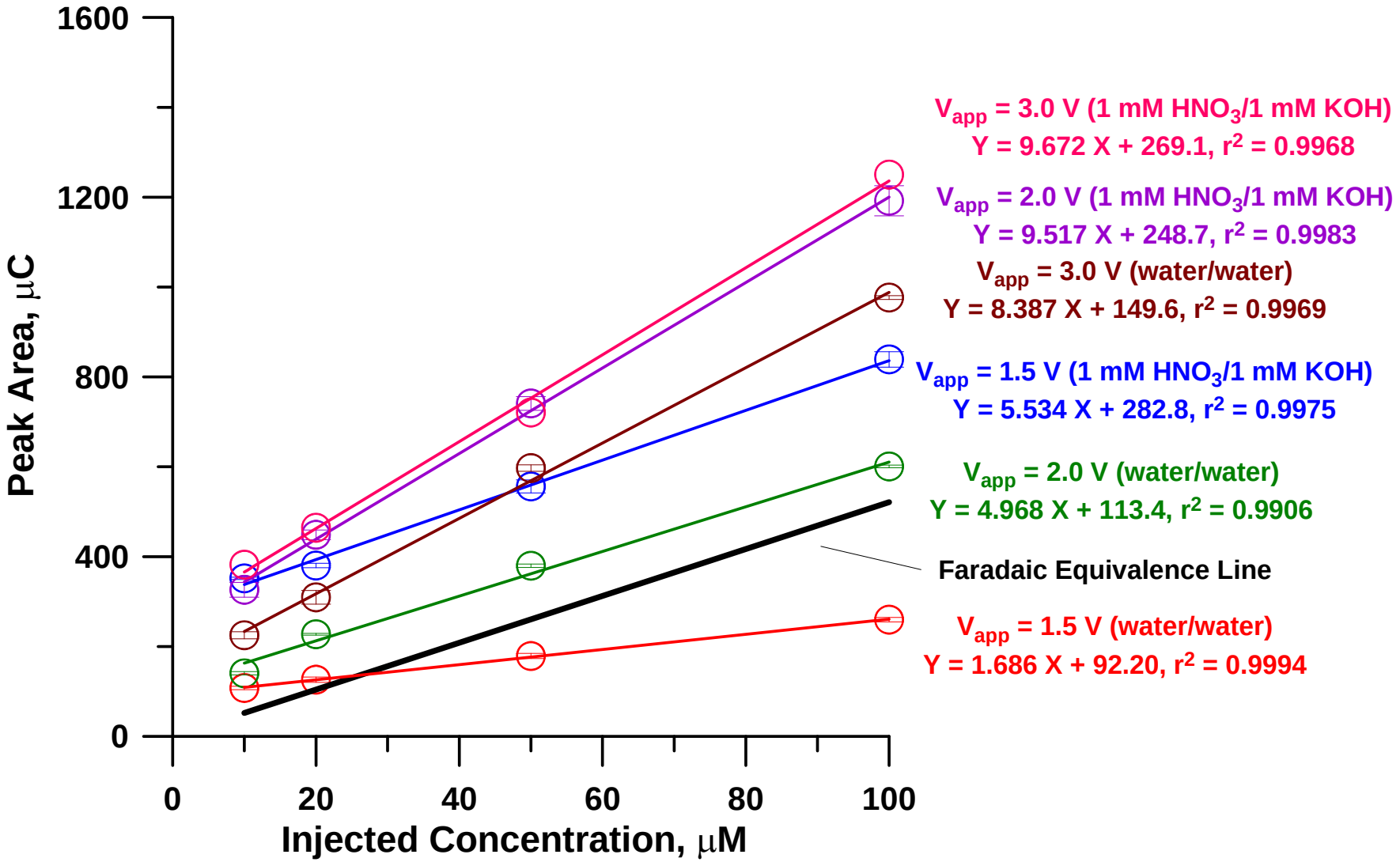

Figure S9. Linear behavior in the 10-100 μM concentration range.

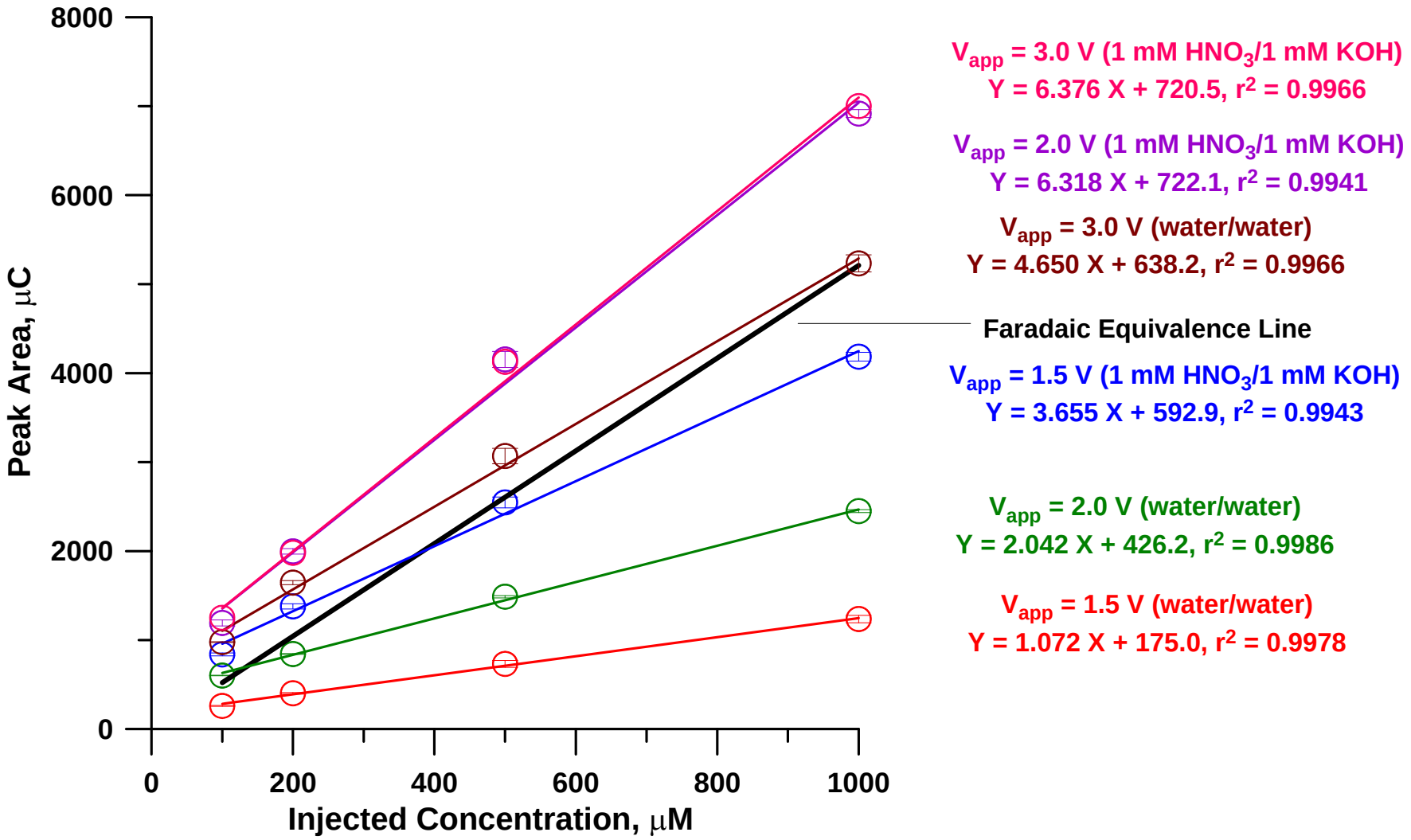

Figure S10. Linear behavior in the 100-1000 μM concentration range. Note the decrease in slope from the previous figure.

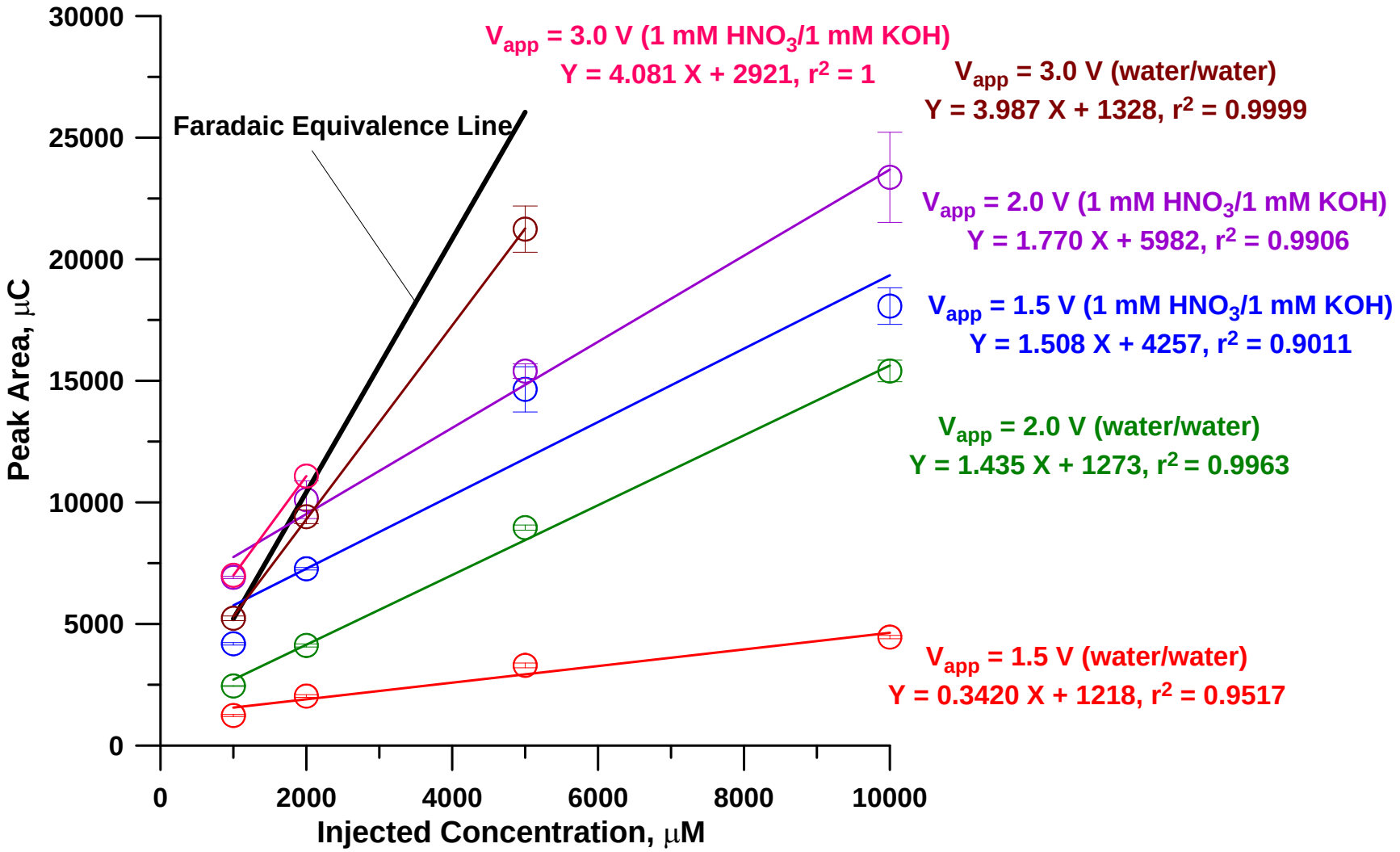

Figure S11. Linear behavior in the 1-10 mM concentration range. Note the decrease in slope from the previous two figures.

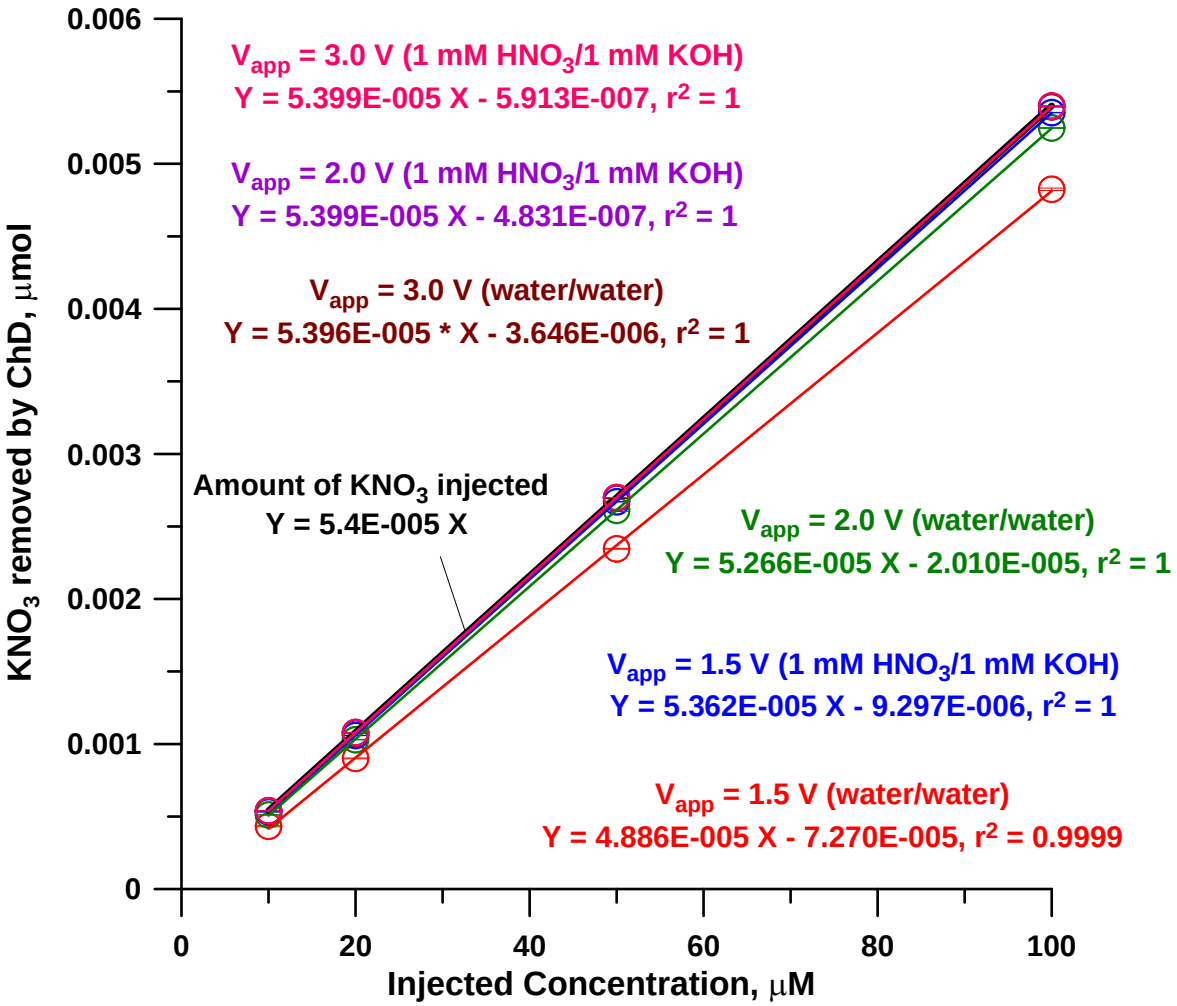

Figure S12. This is the same data as in Figure S9. The ordinate is not the peak area but the amount removed by the ChD as measured by the ratio of the response of two calibrated conductivity detectors (measured in terms of peak area) one placed before and the other after the ChD. The amount removed generally decreases with increasing concentration and decreasing $V_{app.}$ At V_{app} =1.5 V (w/w), 87-94% of the injected amount is removed (except at 10 and 20 mM analyte concentrations, when 83 and 69% are respectively removed); at V_{app} =2.0 V (w/w), 95-98% is removed (except 92.4 and 86% are respectively removed at 10 and 20 mM analyte concentrations), at V_{app} = 3.0V (w/w), 99.4-99.9% is removed across the entire concentration range. Note that instead of water, when acid/base is present in the outer channels, the fraction removed is greatly increased at a given V_{app}. V_{app} = 2.0 V (1 mM HNO_3/1 mM KOH) and V_{app} = 3.0 V (1 mM HNO_3/1 mM KOH), more than 99.9% were removed at the whole concentration range up to 20 mM; except for V_{app} = 1.5 V (1 mM HNO_3/1 mM KOH), 98.0-99.5 % were removed, which is still much higher than V_{app} =2.0 V (w/w).

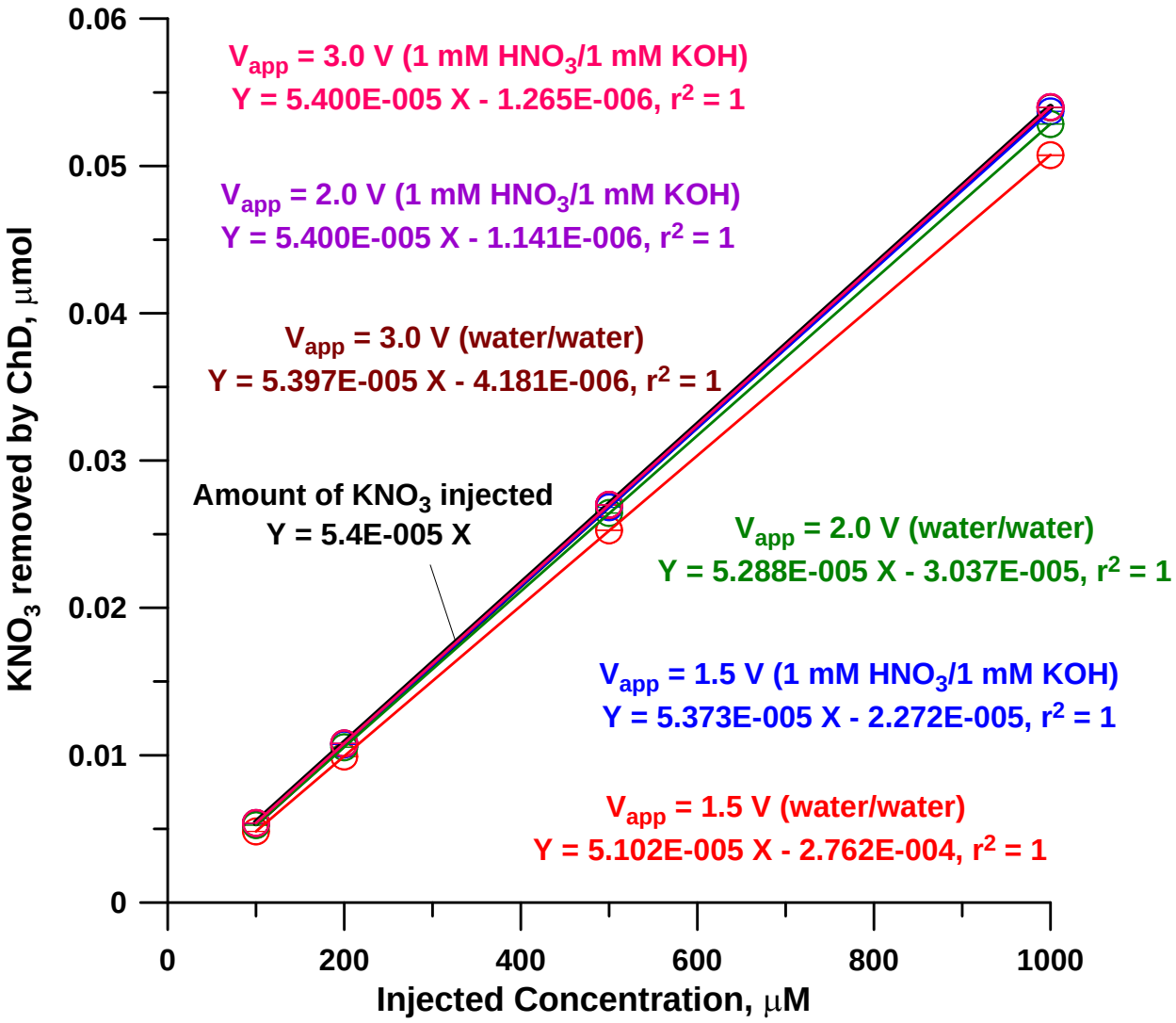

Figure S13. As in Figure S12, 100-1000 μM concentration range.

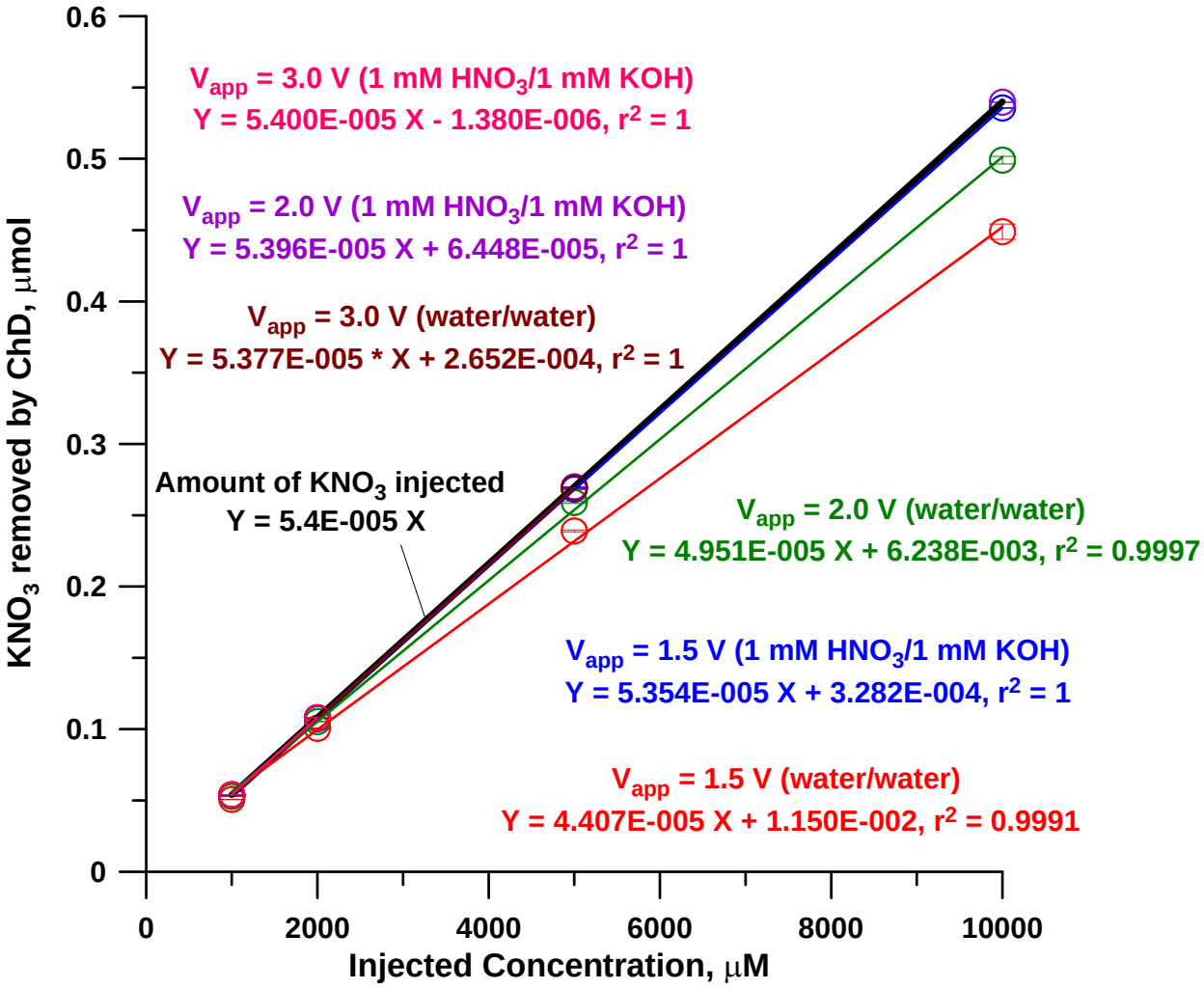

Figure S14. As in Figure S12 and S13, 1-10 mM concentration range.

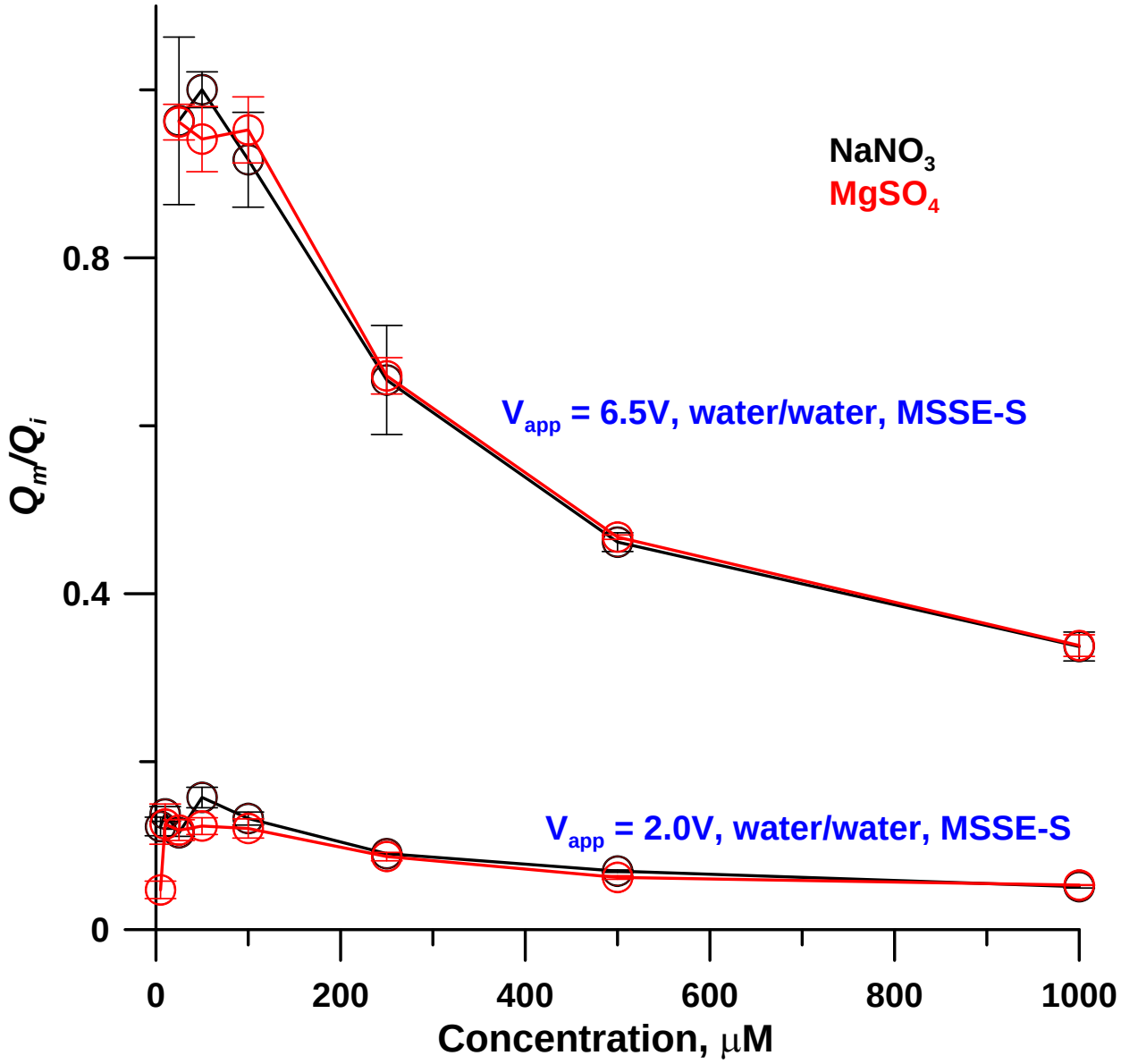

Figure S15. In MSSE devices operated with water in the outer channels, the response decreases with increasing concentration even at low concentrations.

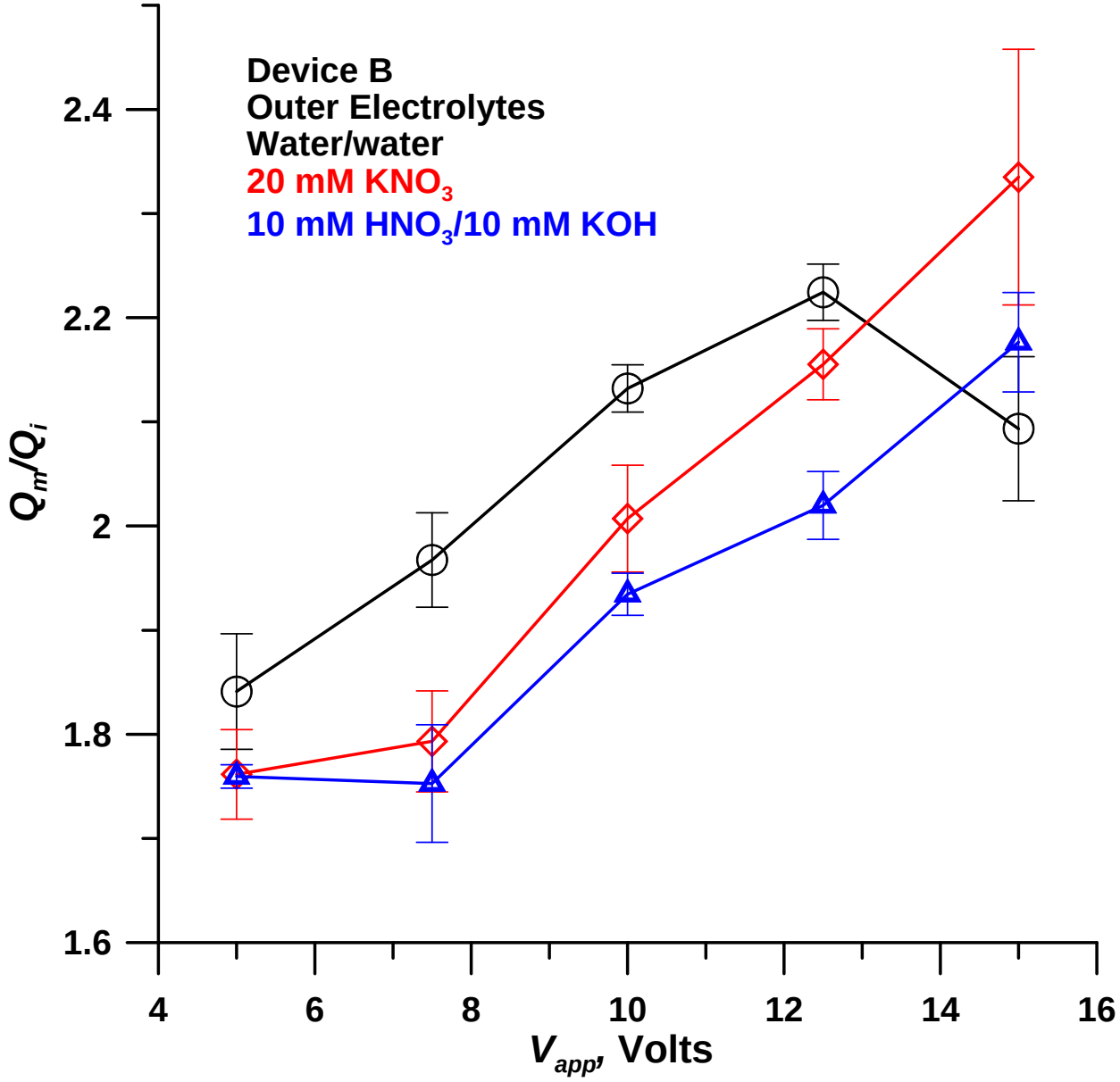

Figure S16. Device ChD-B. Q_m/Q_i shows a maximum value with V_{app} when operated with water/water in the outer channels but not when electrolytes are present. Analyte 2.5 μL 100 μM HCl, CCFR 20 μL/min.

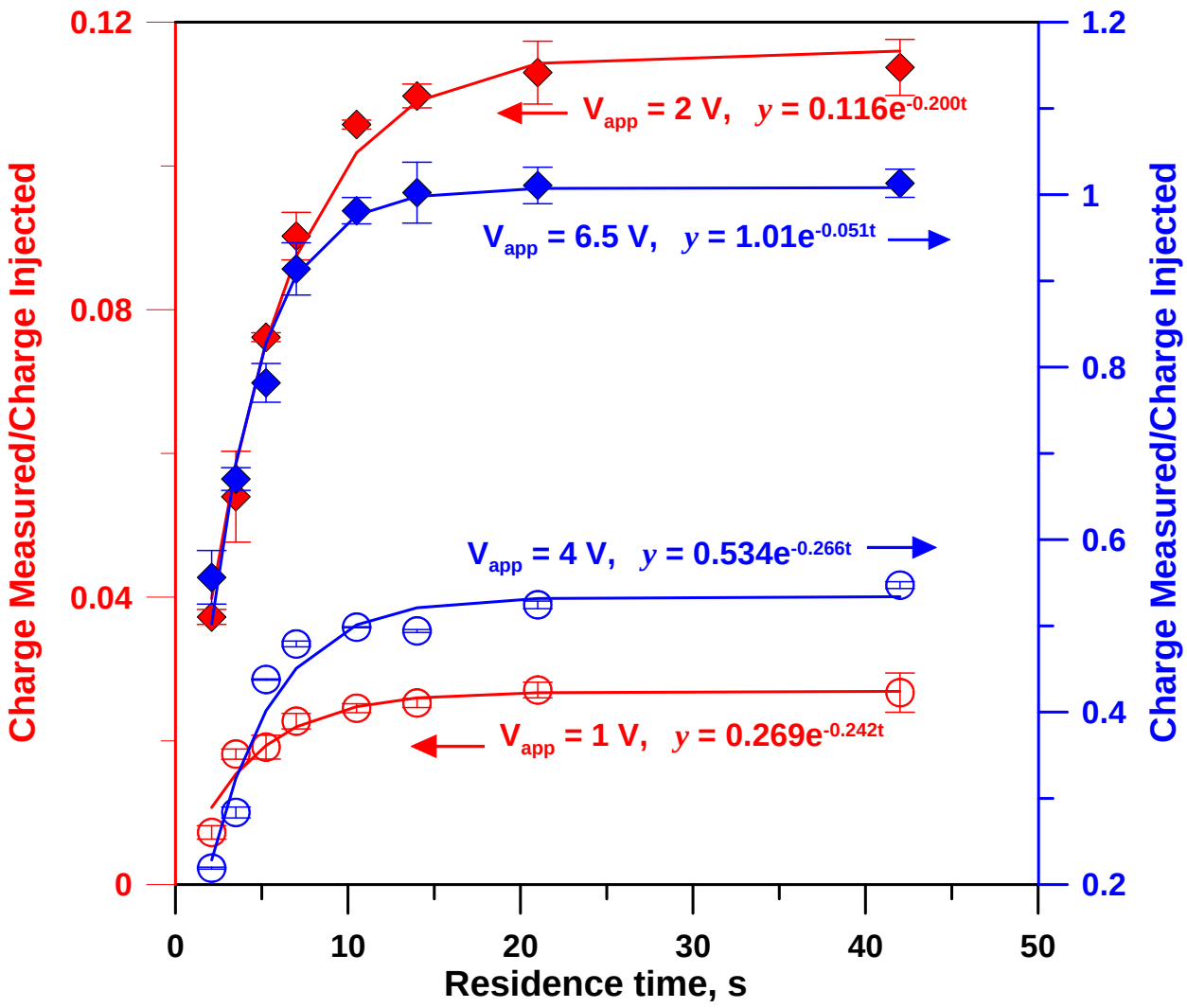

Figure S17. Charge signal injected charge ratio (26.4 μL of 50 μM KNO_3) at 4 different applied voltages as a function of residence time in the device. Device MSSE-S, internal volume 35 μL, central channel flow rates from 50 -1000 μL/min. Both outer channel electrolytes: water, 1.5 mL/min. All solid lines are first order fits in time, the best fit equations are indicated.

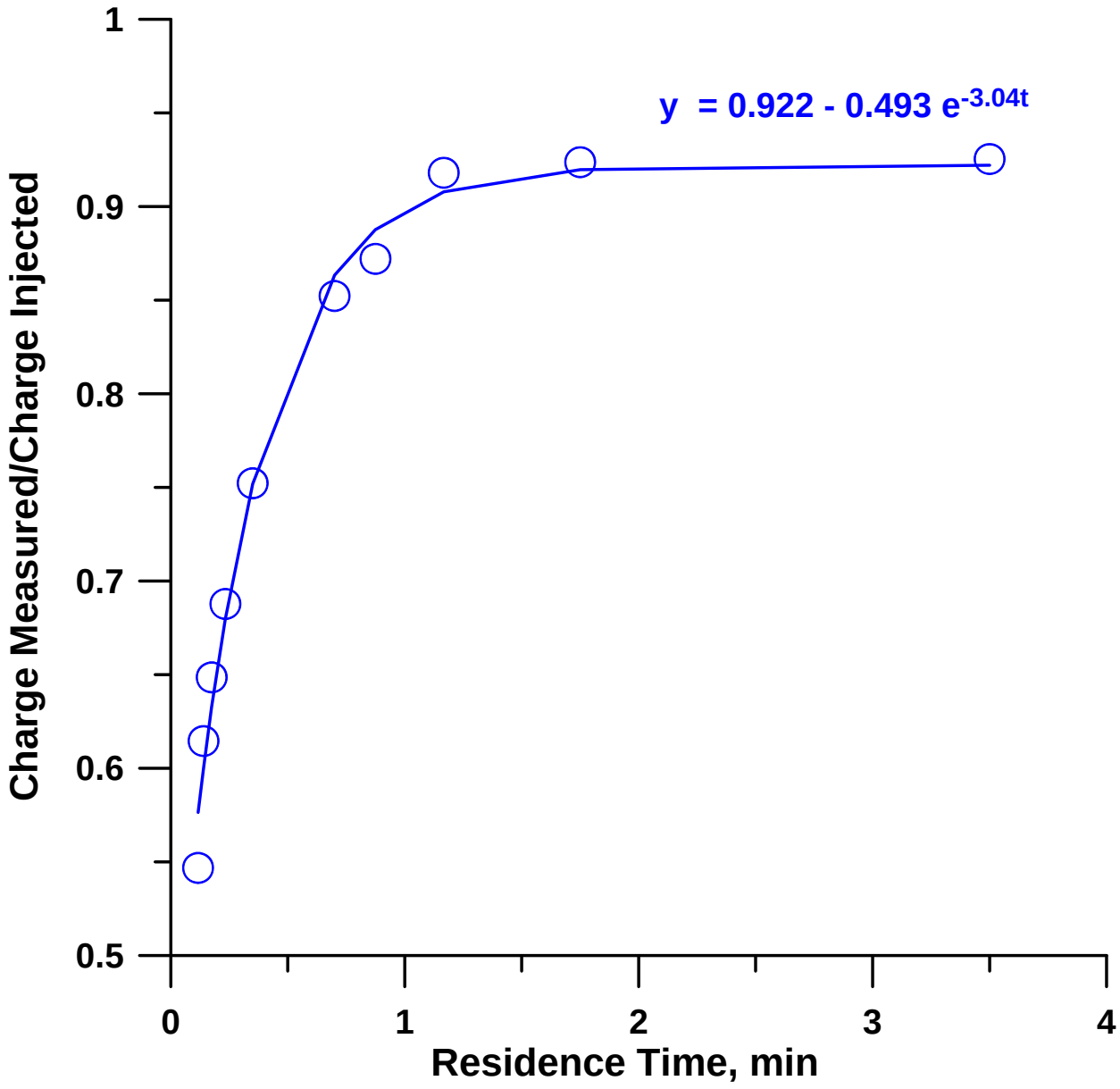

Figure S18. Ratio of the measured charge signal to the injected charge (54.0 μL of 100 μM KNO_3) at 2 V as a function of residence time in the device. Device MAE-S, internal volume 35 μL, central channel flow rates from 100 -3000 μL/min. Outer channel electrolytes: water, 1.5 mL/min. The solid line is first order fit in residence time, the best fit equation is indicated.

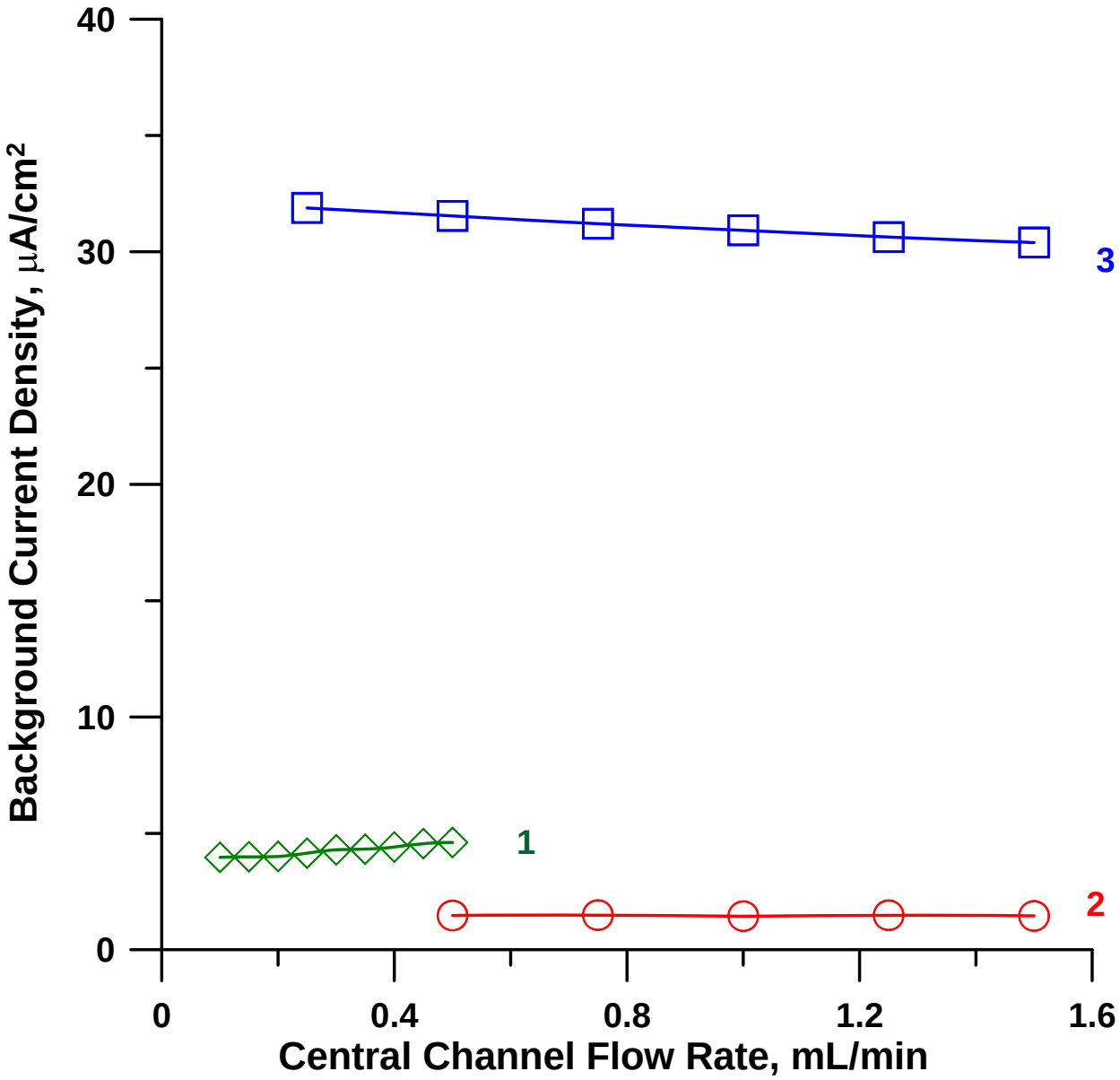

Figure S19. Background current density as a function of water flow rate in the central channel. (1) MSSE-S, water/water; (2) MSSE-L, water/water; (3) MAE-L, water/water. Applied voltage: 2 V; flow rate in the outer channel: 1.5 mL/min for MSSE–S device, 2.0 mL/min for –L devices.

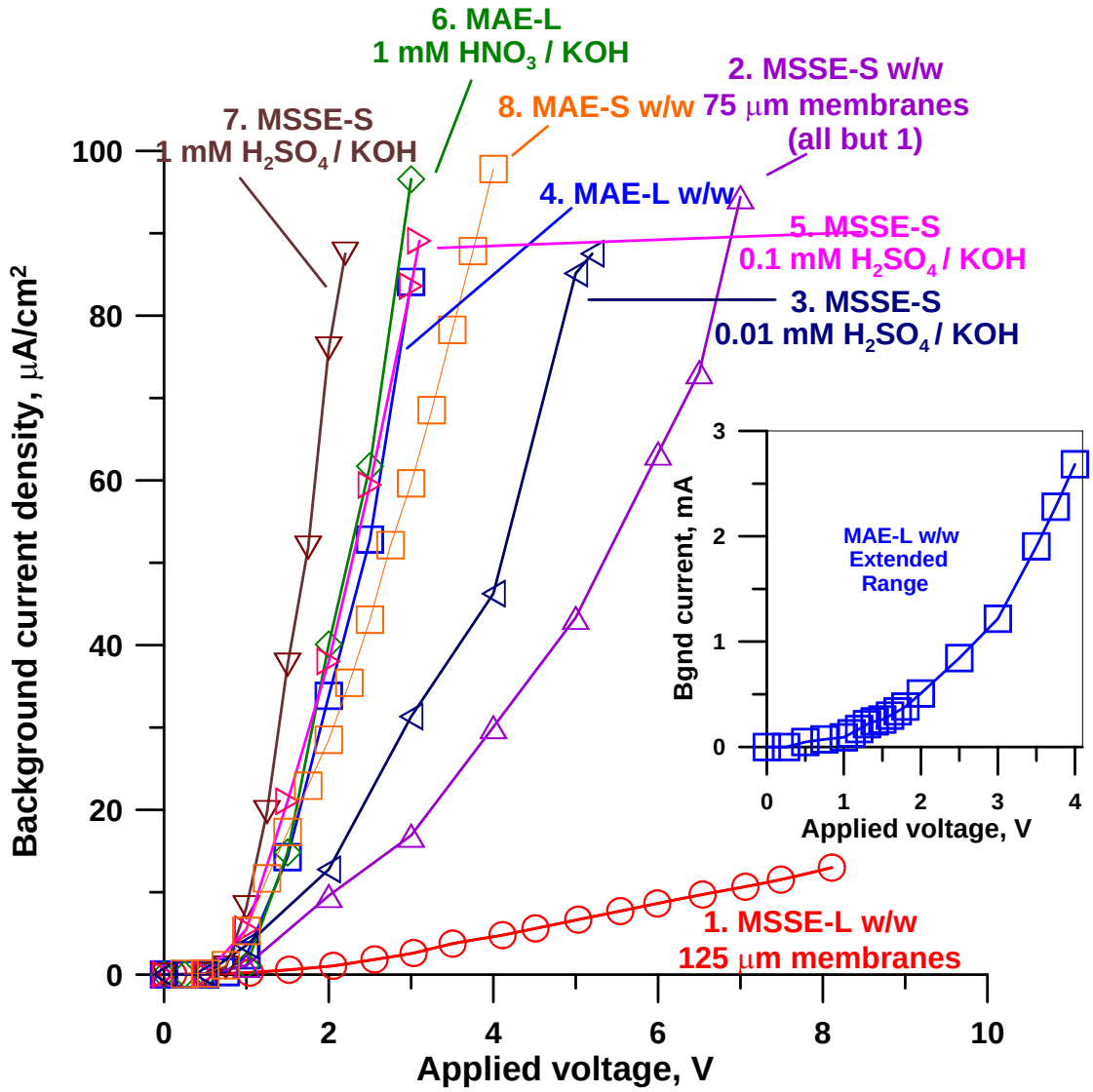

Figure S20. Background current density as a function of applied voltage (reversed bias charge detector operation mode). Devices as indicated. Device 1 used 125 μm thick membranes, all others used 75 μm thick membranes. Water is indicated by w. Central channel: water at 1.00 and 0.20 mL/min for –L and -S devices, respectively; outer channel flow rates ~1.5 mL/min for all devices.

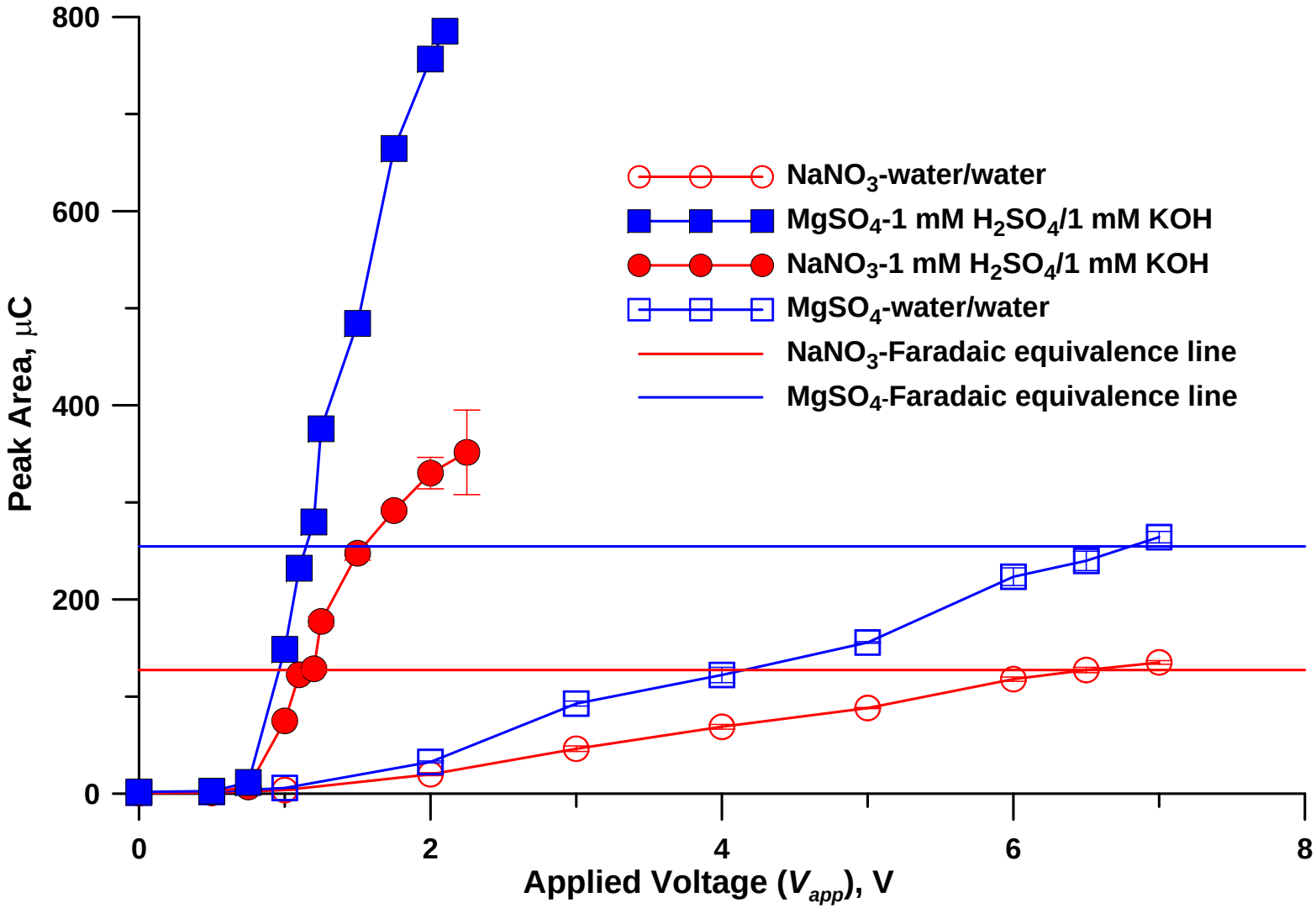

Figure S21. Effect of strong electrolytes (acid and base) in the outer compartments on peak area as a function of applied voltage of a MSSE-S device. Flow in the central channel: water, 0.20 mL/min; flow in the outer channel: water or 1 mM H_2SO_4 on the CEM side and 1 mM KOH on the AEM side, 1.5 mL/min; injected sample: 50 μM $NaNO_3$ and 50 μM $MgSO_4$; injection volume: 26.4 μL. The Faradaic equivalence value is the charge carried by the electrolyte injected. Error bar indicates standard deviation (n = 4).

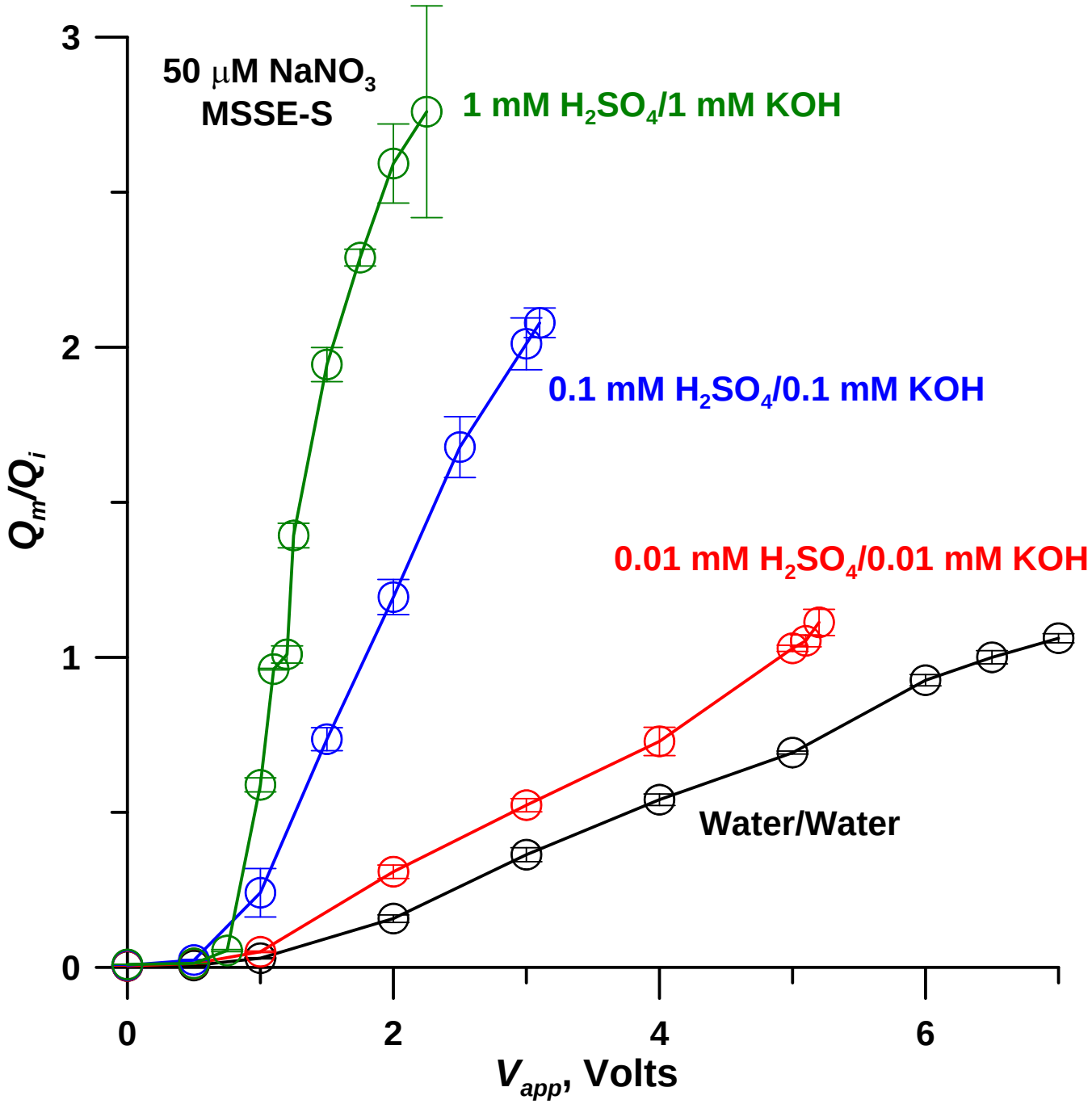

Figure S22. Behavior of a MSSE-S device with different electrolytes in the outer channel and 26.4 μL 50 μM $NaNO_3$ injected. Flow in the central channel: water, 0.20 mL/min; flow in the outer channels: 1.5 mL/min.

Table S1. Signal to noise ratio of a MAE-L device operated with water/water or 1 mM HNO_3/1 mM KOH in the outer channels at three different voltages.

Applied voltage (CEM/AEM)	Signal, µA	Noise, µA	S/N
1.5 V (water/water)	33.0	0.0225	1470
2.0 V (water/water)	66.5	0.0283	2350
3.0 V (water/water)	139	0.232	600
1.5 V (HNO_3/KOH)	107	0.049	2180
2.0 V (HNO_3/KOH)	148	0.0592	2500
3.0 V (HNO_3/KOH)	178	0.296	600

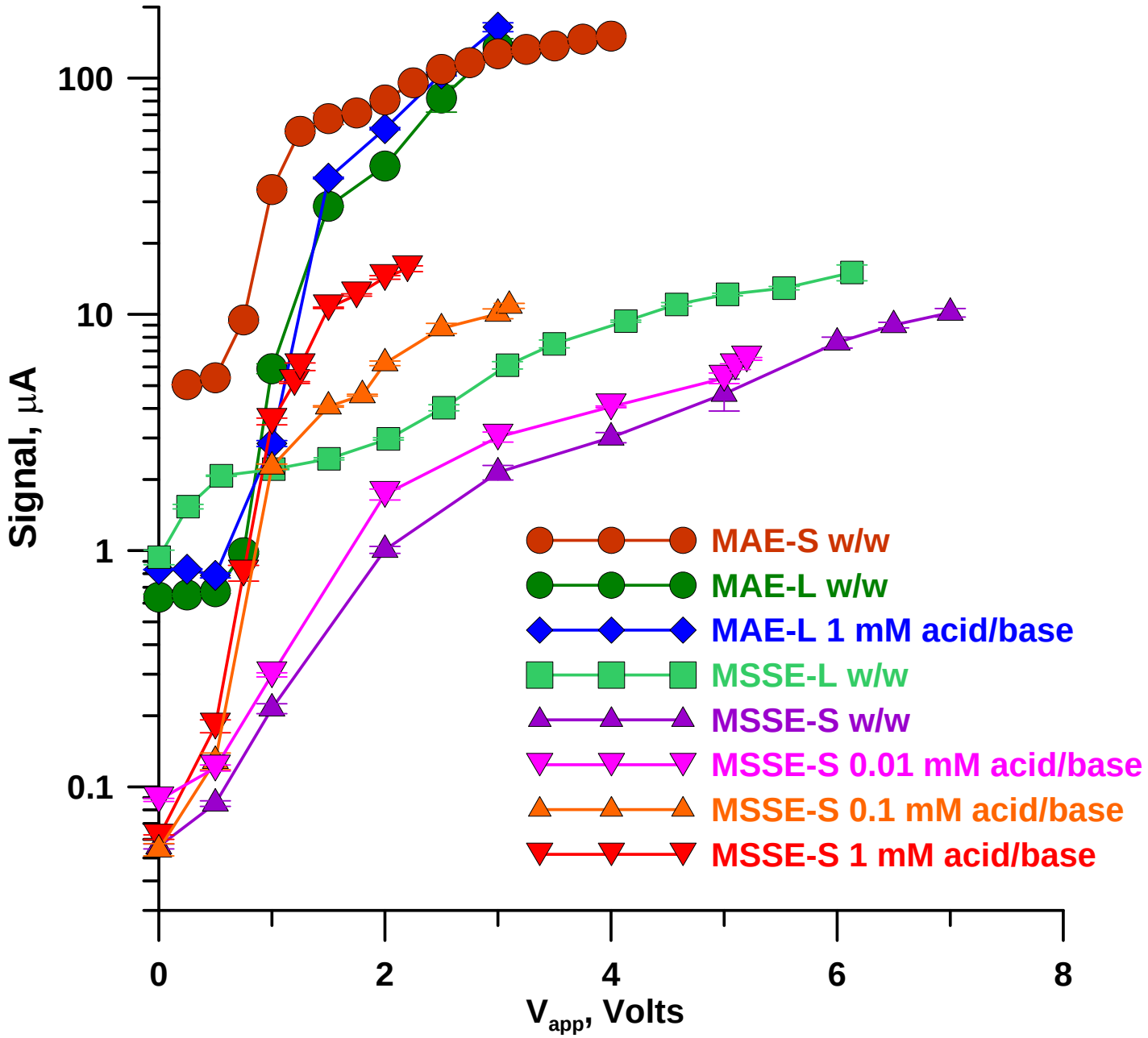

Figure S23. Signal height in μA shown in logarithmic ordinates for various MAE and MSSE devices operated with CEM/AEM channels water/water or acid/ base. For acid 0.01, 0.1, or 1.0 mM H_2SO_4 was used, the same molar concentrations of KOH was used as the corresponding base. Injection volumes of 50 μM $NaNO_3$ were 54 and 26 μL, respectively, for type -L and –S devices. Central channel flow rates were 1000 and 200 μL/min, respectively for type -L and –S devices. See Figure S5 for depiction of these data in a linear ordinate scale.

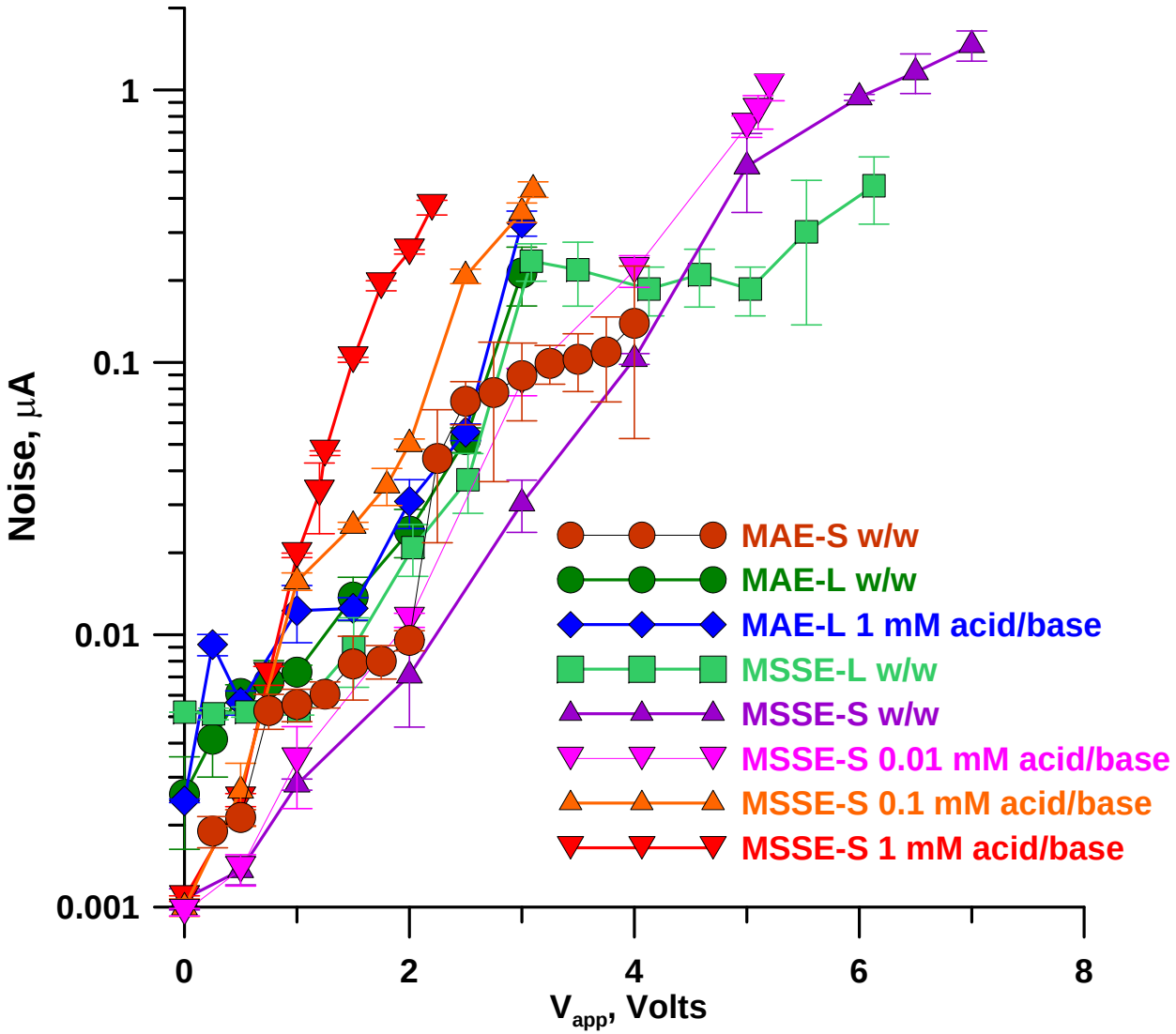

Figure S24. Background noise in experiments described in Figure S23; logarithmic ordinate. For a linear ordinate see Figure S6.

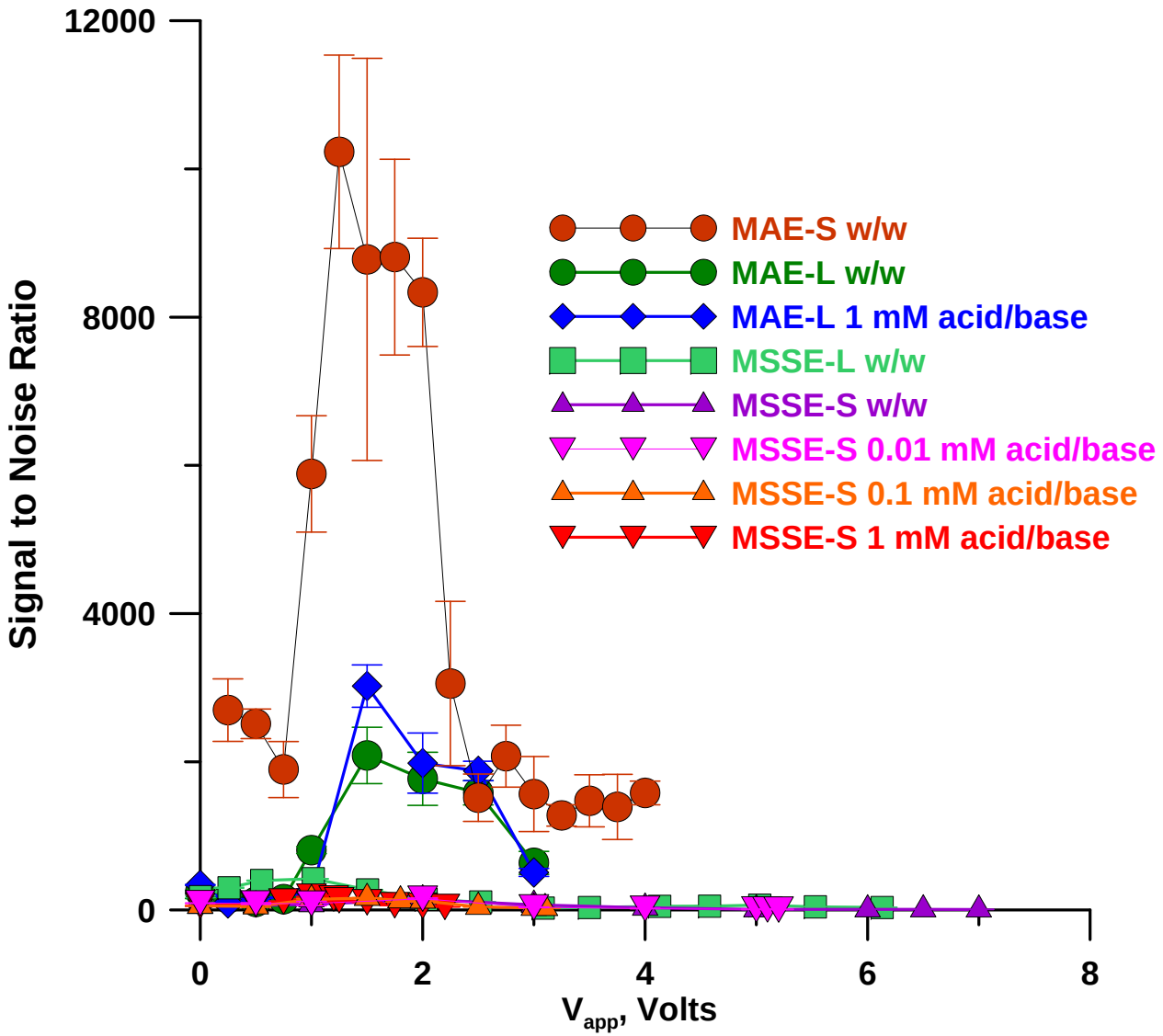

Figure S25. The data in Figure 9 plotted with a linear ordinate.

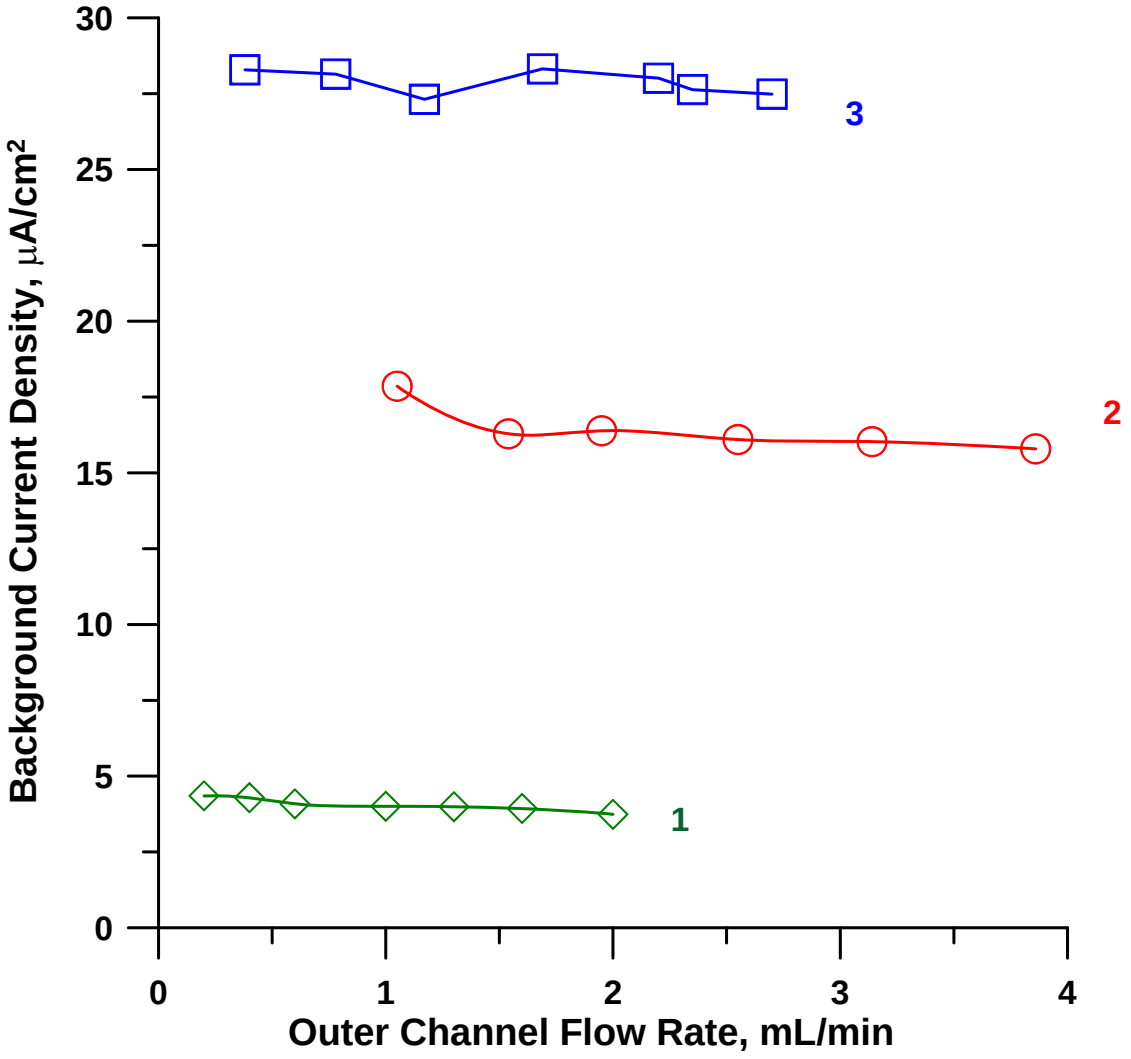

Figure S26. . Background current density as a function of flow rate in the outer channel**.** (1) MSSE-S, water/water; (2) MSSE-L, water/water; (3) MAE-L, water/water. Applied voltage: 2 V; flow rate in the central channel: 0.20 mL/min for the –S devices, 1.00 mL/min for both -L devices. What little change is observed relates to purity of the water actually entering the outer channel of the devices. It is difficult to prevent CO_2 intrusion to the water flowing in the connecting tubing between the water sources and the device inlet. At slower flow rates, the residence time of the water in the interconnecting tubing is higher and effectively the CO_2 content of the water reaching the outer channels of the device is higher. In MSSE devices this reduces the voltage drop in the outer channels. Some of the CO_2 can also permeate through the membranes into the central channel, ionize and then be removed by the normal operation of the device, contributing to background current.

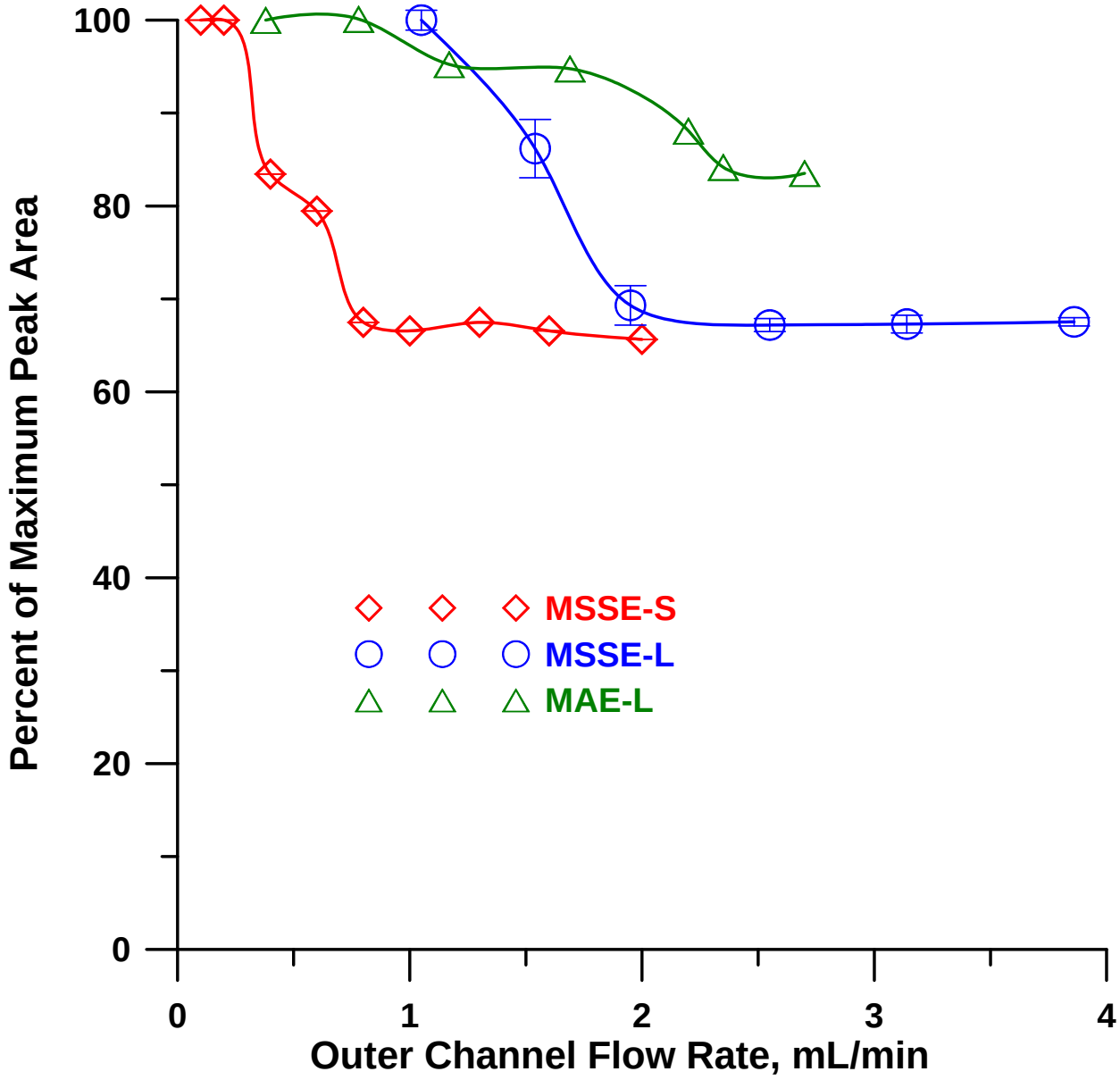

Figure S27. The dependence of the observed charge signal (Q_m) on the outer channel flow rates. All devices operated water/water and both outer channels had the same flow rate. Central channel flow rates were 0.20 and 1.00 mL/min, respectively for –S and –L devices. Analyte 50 μM KNO_3, 26 and 54 μL, respectively, for –S and -L devices.

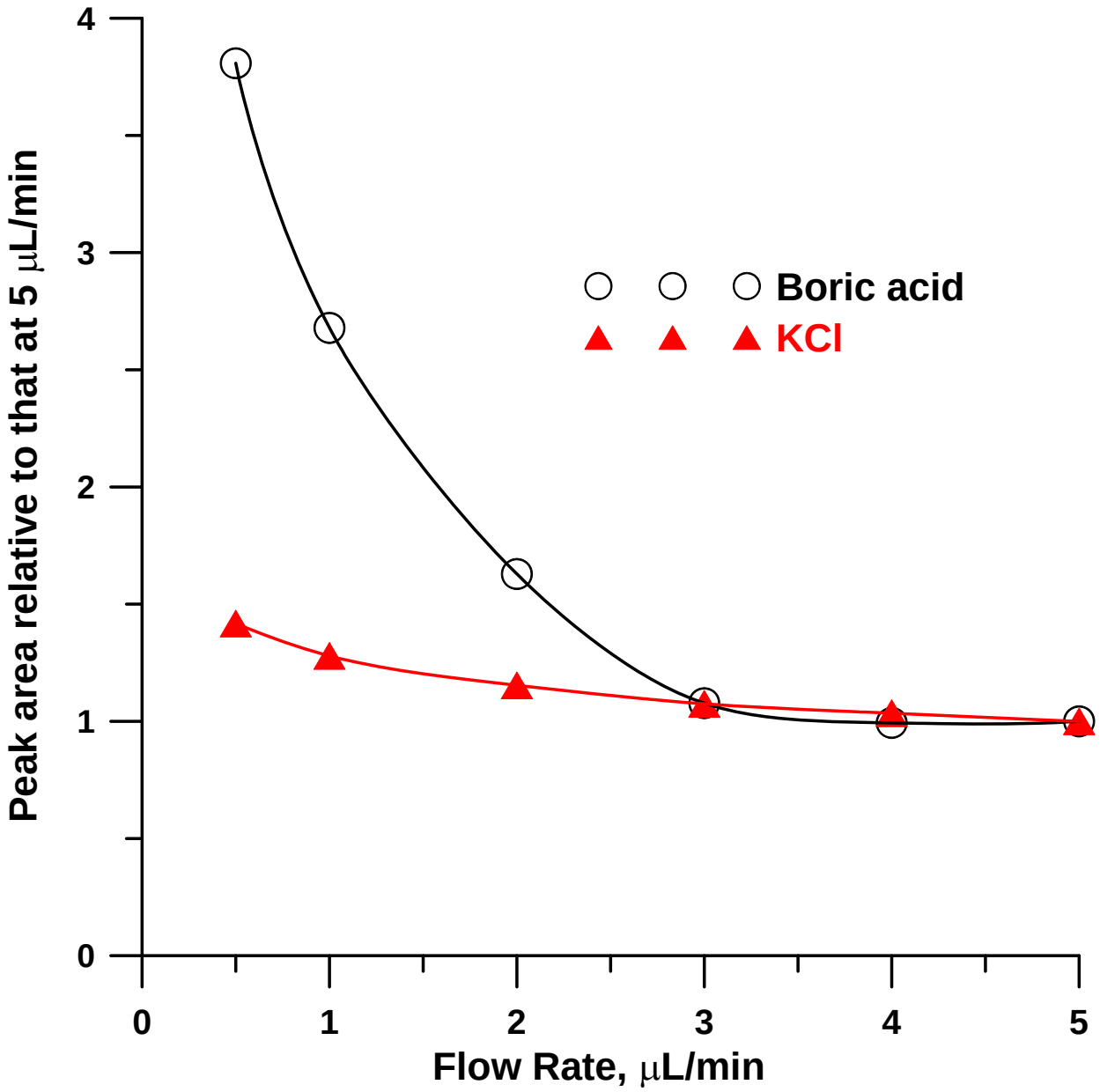

Figure S28. Charge detector (Device ChD-B) signal as a function of flow rate. Applied voltage 14 V, 2.5 nmol each of KCl and boric acid are injected.

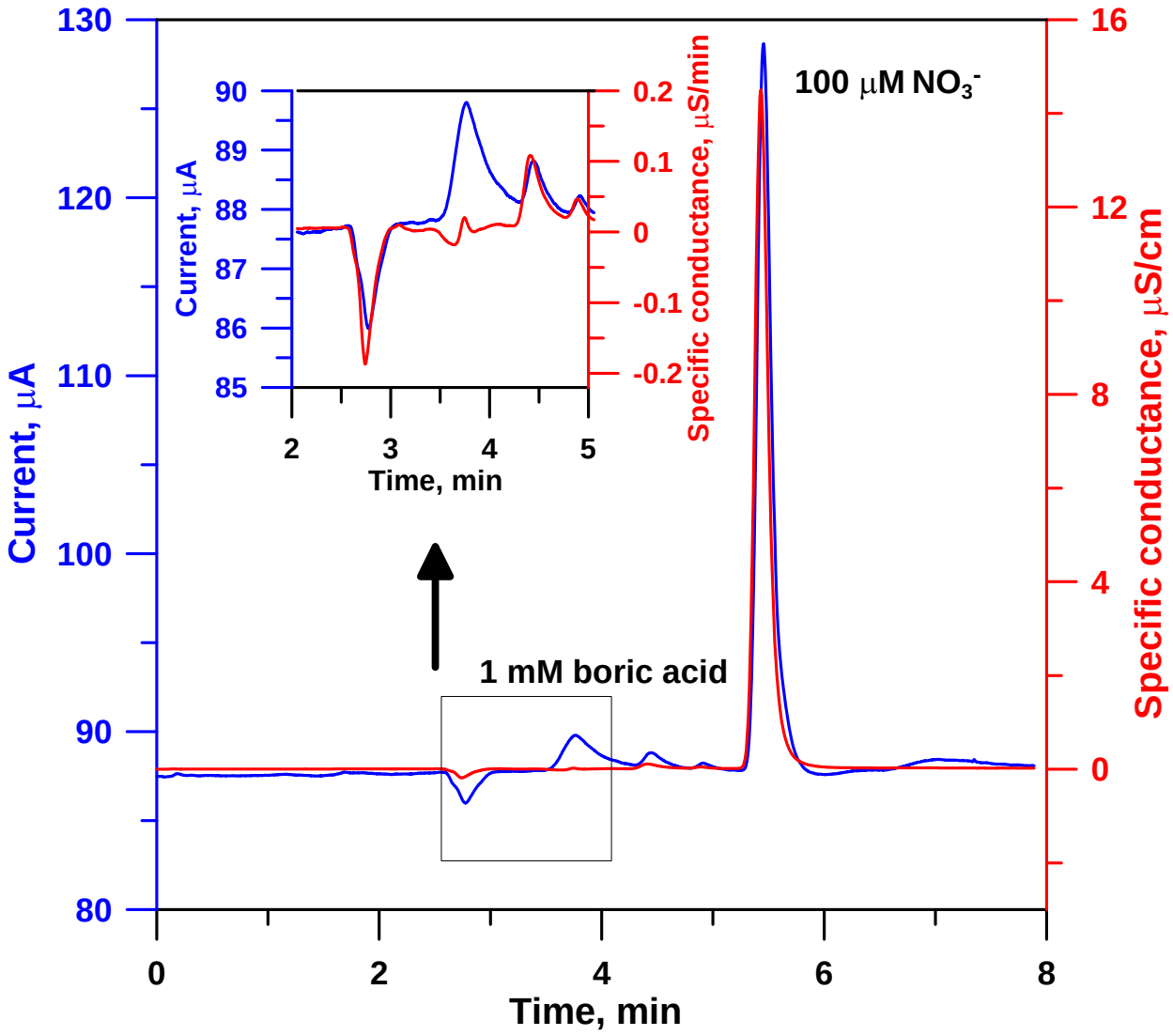

Figure S29. Chromatograms by serial conductivity detector (CD 25) followed by MAE-S ChD V_{app} = 2 V (outer channels water @ 1.5 mL/min). GS-50 .pump pumping 25 mM electrogenerated KOH @ 1 mL/min, AG11-HC (4 x 50 mm)/AS 11-HC (4 x 250 mm) columns, 35 °C (LC-30 oven), ASRS Ultra-II suppressor (all from Dionex). Analyte concentrations 100 μM KNO_3 and 1 mM boric acid. The inset shows a much higher signal for boric acid obtained with ChD than CD.

GLOSSARY

AEM: Anion Exchange Membrane

BIM: Bipolar Ion Exchange Membrane

CCFR: Central Channel Flow Rate

CD: Conductivity Detector

CEM: Cation Exchange Membrane

ChD: Charge Detector, as described in this paper

ChD-B: Ion exchange resin bead based charge detector

ChD-M: Ion exchange membrane based charge detector

IC: Ion Chromatography

IEM: Ion Exchange Membrane

MAE: A ChD-M devices with adjacent electrodes, electrodes are in contact with the membrane, the larger and smaller scale devices (MAE-L, MAE-S) have active membrane areas of 14 and 3.6 cm^2), respectively

MSSE: A ChD-M device with the electrodes separated from the membranes by a screen. Also built with large (-L) and small (-S) membrane areas, as above

Q_m: Measured charge response, peak area in coulombs

Q_i: Total charge in coulombs injected into the system, based on the amount of the strong electrolyte injected in moles

V_{app}: Total voltage applied across a device

w/w: Refers to the two outer channels being operated with water and water

LITERATURE CITED

(1) Stillian, J. *LC-GC Mag*. **1985,** *3,* 802-812.
(2) Rabin, S.; Stillian, J.; Barreto, V., Friedman, K.; Toofan, M. *J. Chromatogr.,* **1993**, *640,* 97-109.
(3) Pohl, C.; Slingsby, R. W.; Stillian, J. R.; Gajek, R. US Patent 4,99,098. March 12, 1991.
(4) Stillian, J. R.; Barreto, V. M.; Friedman, K. A.; Rabin, S. B.; Mahmood, T. US Patent 5,352,360. October 4, 1994.
(5) Haddad, P. R.; Jackson, P. E.; Shaw, M. J. *J. Chromatogr. A.* **2003,** *1000,* 725-742.
(6) Liu, Y.; Srinivasan, K.; Pohl, C.; Avdalovic, N. *J. Biochem. Biophys. Methods* **2004,** *60,* 205–232.
(7) Dasgupta, P. K. in *Ion Chromatography*, Tarter, J. G., Ed., Marcel Dekker, 1987. pp 220-224.